International Journal of Solids and Structures 52 (2015) 56–71

Contents lists available at ScienceDirect

International Journal of Solids and Structures

journal homepage: www.elsevier.com/locate/ijsolstr

# Green's functions and extended displacement discontinuity method for interfacial cracks in three-dimensional transversely isotropic magneto-electro-elastic bi-materials

YanFei Zhao [a], MingHao Zhao [b], Ernian Pan [a], CuiYing Fan [b,*]

[a] Department of Civil Engineering, University of Akron, Akron, OH 44325, USA
[b] Henan Key Engineering Laboratory for Anti-Fatigue Manufacturing Technology and School of Mechanical Engineering, Zhengzhou University, Zhengzhou, Henan 450001, China

ARTICLE INFO

*Article history:*
Received 12 March 2014
Received in revised form 18 September 2014
Available online 2 October 2014

*Keywords:*
Magneto-electro-elastic bi-materials
Interfacial crack
Extended displacement discontinuity method
Electrically and magnetically impermeable
Gaussian distribution function

ABSTRACT

In this paper, we derive the Green's functions of constant extended interfacial displacement discontinuities within a rectangular element and of point extended interfacial displacement discontinuities in three-dimensional transversely isotropic magneto-electro-elastic (MEE) bi-materials. The derived Green's functions along with the extended displacement discontinuity method are applied to analyze the electrically and magnetically impermeable interfacial cracks in the three-dimensional MEE bi-materials. To deal with the oscillatory singularities at the crack front, the Dirac delta function in the Green's functions is replaced by the Gaussian distribution function, and correspondingly, the unit Heaviside function is approximated by the Error function. Numerical study illustrates the effect of the $\varepsilon$ parameter in the Gaussian distribution function on the *J*-integral. The stress intensity factors, electric displacement intensity factor, and magnetic induction intensity factor are expressed in terms of the extended displacement discontinuities. The influence of different MEE material mismatches as well as different extended loadings (uniformly or non-uniformly distributed on the crack face) on the fracture parameters is investigated. Different rectangular crack sizes are also considered in the numerical simulation.



## 1. Introduction

Since Williams (1959) first investigated a semi-infinite interfacial crack in elastic dissimilar media, increasing enthusiasm follows in studying the behaviors and characters of interfacial cracks. The oscillatory singularity at the two-dimensional (2D) interfacial crack tip was discussed (Erdogan, 1965; England, 1965; Rice and Sih, 1965; Suo and Hutchinson, 1990) and different approaches were proposed to deal with this unsatisfactory oscillatory behavior (e.g., Atkinson, 1977; Comninou, 1977, 1990; Dundurs and Gautesen, 1988). Related works on the corresponding three-dimensional (3D) interfacial fracture problems can be found in Willis (1971), Lazarus and Leblond (1998a,b), Antipov (1999), Bercial-Veleza et al. (2005) and Pindra et al. (2008), among others. One efficient way of simulating interfacial cracks is by interfacial dislocations (Eshelby, 1951; Comninou, 1977; Qu and Li, 1991). But the oscillating singularity would still exist with the Dirac delta function in the solutions. Mathematically, it has been proved that a variety of appropriate approximations of the Dirac delta function can be made depending on the specific physical or engineering problems under consideration. Zhang and Wang (2013) reconsidered the dislocation approach for interfacial cracks and replaced the Dirac delta function with the Gaussian distribution function to eliminate the oscillatory singularity.

The analysis of the elastic interfacial cracks was then extended to the piezoelectric bi-material (Kuo and Barnett, 1991; Suo et al., 1992; Beom and Atluri, 1996; Qin and Mai, 1999; Herrmann and Loboda, 2000; Zhao et al., 2008b). One of the most interesting findings from these studies was that besides the classical singularity $r^{-1/2}$ and the well-known oscillatory singularity $r^{-1/2\pm i\varepsilon}$, the extended stresses have a new type of singularity $r^{-1/2\pm\kappa}$ near the crack tip in 2D and also in 3D piezoelectric bi-materials. It was also found that an impermeable interfacial crack in the transversely isotropic bi-materials could be classified into two types according to the feature of the $\varepsilon$-singularity and $\kappa$-singularity of the stress field near the crack tip.

The first magneto-electro-elastic (MEE) composite was fabricated by Van Run et al. (1974). In recent two decades, due to the interesting coupling features among the mechanical, electrical

* Corresponding author at: The School of Mechanical Engineering, Zhengzhou University, No. 100 Science Avenue, Zhengzhou, Henan Province 450001, China. Tel.: +86 371 67781832.
*E-mail address:* fancy@zzu.edu.cn (C. Fan).

http://dx.doi.org/10.1016/j.ijsolstr.2014.09.018
0020-7683/

and magnetic fields, MEE composites have attracted extensive attentions from different branches of science and engineering. Since defects may exist in these novel composites, fracture problems in them need to be addressed. Representative contributions in this direction include 2D in-plane fracture problems (Song and Sih, 2003; Sih and Song, 2003; Gao et al., 2003; Wang and Mai, 2003) and anti-plane problems (Wang and Shen, 1996; Spyropoulos et al., 2003; Gao et al., 2004; Chue and Liu, 2005; Zhong and Li, 2006; Hu and Chen, 2014).

For the study of the crack problems in MEE bi-materials, all the previous works, such as Gao et al. (2003), Zhou et al. (2004) and Tian and Gabbert 2005, helped shed light on the understanding of 2D interfacial fracture behaviors of MEE bi-materials. The study on the corresponding 3D interfacial fracture problems is more important in theory and practical in engineering applications. In this direction, Zhao et al. (2008a) analyzed the interfacial crack of an arbitrary shape in 3D transversely isotropic MEE bi-materials by extending their 3D piezoelectric bi-material approach (Zhao et al., 2008b). They found that as its counterpart in piezoelectric bi-materials, the stress near the crack front in MEE bi-material also has two kinds of singularity, namely, the oscillating and non-oscillating singularities, depending on the specific MEE bi-material system. They further explained that these two singularities cannot coexist in the same bi-material system. Zhu et al. (2009) adopted the integro-differential equation method to analyze the 3D interfacial crack in MEE bi-material. In their work, the unknown displacement discontinuities along the crack face were approximated by the product of extended basic density functions and polynomials and the resulting integro-differential equations were solved numerically.

The displacement discontinuity method was first proposed by Crouch (1976) to study the crack problems in elasticity numerically. Later studies showed that this method is efficient and flexible, and further can be conveniently applied to analyze 3D crack problems in piezoelectric media (Zhao et al., 1997) and in MEE materials (Zhao et al., 2007) by extending the original elastic displacement discontinuity to include the piezoelectric potential and magnetic potential.

In this paper, we first apply the boundary integro-differential method (i.e., Zhao et al., 2008a) to derive the Green's functions of the extended interfacial displacement discontinuities in 3D transversely isotropic MEE bi-material. The Dirac delta function in the Green's function is then approximated by the Gaussian distribution function as in Zhao et al. (2014) to remove the oscillatory singularities. Correspondingly, the approximation of the unit Heaviside function is introduced based on its relation with the Dirac delta function. Using the obtained 3D Green's functions, the extended displacement discontinuity method is applied to analyze the interfacial cracks in 3D MEE bi-materials.

This paper is organized as follows: Section 2 outlines the basic equations of the MEE material. In Section 3, solutions, especially those on the interface, for an interfacial crack in 3D MEE bi-material are obtained via the integro-differential approach which is extended from Zhao et al. (2008a). Then the Green's functions of the constant extended interfacial displacement discontinuities within a rectangular element and the point extended interfacial displacement discontinuities are derived. In Section 4, the Dirac delta function and the unit Heaviside function in the Green's functions are approximated, respectively, by the Gaussian distribution function and the Error function. The analytical expressions for the stress intensity factors, electric displacement intensity factor, magnetic induction intensity factor and the energy release rate are also given. Extended displacement discontinuity method is introduced in Section 5. In Section 6, numerical results are presented to illustrate the effect of the $\varepsilon$ parameter in the Gaussian distribution function on the $J$-integral. The influence of different MEE material mismatches and different extended loadings (uniformly or non-uniformly distributed on the crack face) on the crack parameters is further investigated. Conclusion is drawn in Section 7.

## 2. Basic equations

In a three-dimensional Cartesian coordinate system $x_i$ ($i = 1,2,3$), the governing equations for a linear transversely isotropic MEE medium without body force and free from electric charge and current are given by (1) the equilibrium equation, (2) the kinematic equation, and (3) the constitutive equation as listed below:

$$\sigma_{ij,j} = 0, \quad D_{i,i} = 0, \quad B_{i,i} = 0, \tag{1}$$

$$\varepsilon_{ij} = \frac{1}{2}(u_{i,j} + u_{j,i}), \quad E_i = -\varphi_{,i}, \quad H_i = -\psi_{,i}, \tag{2}$$

$$\begin{aligned} \sigma_{ij} &= c_{ijkl}\varepsilon_{kl} - e_{kij}E_k - f_{kij}H_k, \\ D_i &= e_{ikl}\varepsilon_{kl} + \kappa_{il}E_l + g_{il}H_l, \\ B_i &= f_{ikl}\varepsilon_{kl} + g_{li}E_l + \mu_{il}H_l, \end{aligned} \tag{3}$$

where $\sigma_{ij}$, $D_i$ and $B_i$ are stress, electric displacement and magnetic induction components, respectively, and they are called extended stresses. $u_i$, $\varphi$ and $\psi$ are displacement components, electric potential and magnetic potential and are called extended displacements. $\varepsilon_{ij}$, $E_i$ and $H_i$ denote, respectively, strain components, electric field and magnetic field. $c_{ijkl}$, $e_{ikl}$, $f_{ikl}$, $\kappa_{il}$, $g_{il}$ and $\mu_{il}$ are elastic constants, piezoelectric constants, piezomagnetic constants, dielectric permittivity, electromagnetic constants and magnetic permeability, respectively. A subscript comma denotes the partial differentiation with respect to the coordinate, with repeated indices taking their summation from 1 to 3 (Huang et al., 1998; Pan, 2002; Zhao and Fan, 2008).

## 3. Green's functions of extended interfacial displacement discontinuities

### 3.1. Integro-differential expressions of extended stresses due to an interfacial crack

We consider a transversely isotropic MEE bi-material system with its interface parallel to the plane of isotropy and lies on the $ox_1x_2$-plane, as schematically shown in Fig. 1. The poling direction is along the $x_3$-axis. A flat crack of arbitrary shape lies on the interface. The upper and lower faces of this interfacial crack are denoted, respectively, by $S^+$ and $S^-$ with their outer normal vectors being

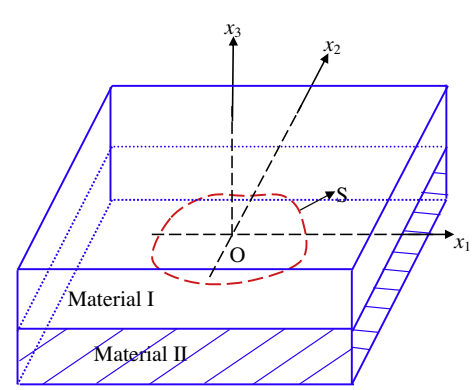


**Fig. 1.** An interfacial crack of an arbitrary shape under extended loadings on its surface in a transversely isotropic MEE bi-material.

$$\{n_i\}^+ = \{0,0,-1\}, \quad \{n_i\}^- = \{0,0,1\}. \tag{4}$$

The electric and magnetic boundary conditions on the crack face can be different (Wang and Mai, 2007; Zhao et al., 2007). In this paper, we assume the electrically and magnetically impermeable condition along the crack face to illustrate our solution procedure. By this assumption, we have $D_3(x_1,x_2,0^+) = D_3(x_1,x_2,0^-) = 0$ and $B_3(x_1,x_2,0^+) = B_3(x_1,x_2,0^-) = 0$.

As we know, one technique of dealing with cracks in an infinite media under far-field loadings is transferring the far-field loadings onto the crack faces. This can be achieved by superposing the crack free problem and the perturbed problem. For the perturbed problem, the loadings applied on the crack faces which are related to the far-field loadings are calculated from the crack free problem. It can be proved that the applied extended tractions (including the tractions $p_i$, the electric displacement boundary value $\omega$, and the magnetic induction boundary value $\gamma$) on the upper and lower crack faces have the same magnitude but opposite directions, i.e.,

$$p_i|_{S^+} = -p_i|_{S^-}, \quad \omega|_{S^+} = -\omega|_{S^-}, \quad \gamma|_{S^+} = -\gamma|_{S^-}, \quad (i = 1,2,3), \tag{5a}$$

where

$$p_i = \sigma_{ij}n_j, \quad \omega = D_i n_i, \quad \gamma = B_i n_i. \tag{5b}$$

Thus, the present interfacial crack under far field loadings is converted to the perturbed problem which is the main focus of this paper.

Using the approach which is similar to the one in Zhao et al. (2008a), the displacement components $u_i$, the electric potential $\varphi$ and the magnetic potential $\psi$ at point $(x_1,x_2,h)$ induced by an arbitrary interior crack on the plane $x_3 = h$ are expressed by the following integral over the crack face $S(\xi,\eta;h)$:

$$\begin{aligned} u_i(x_1,x_2,h) &= -\int_{S^+}\left[P_{ij}^F\|u_j\| + \Omega_i^F\|\varphi\| + \Gamma_i^F\|\psi\|\right]dS, \\ \varphi(x_1,x_2,h) &= \int_{S^+}\left[P_j^D\|u_j\| + \Omega^D\|\varphi\| + \Gamma^D\|\psi\|\right]dS, \quad i = 1,2,3, \\ \psi(x_1,x_2,h) &= \int_{S^+}\left[P_j^B\|u_j\| + \Omega^B\|\varphi\| + \Gamma^B\|\psi\|\right]dS, \end{aligned} \tag{6}$$

where $P$, $\Omega$ and $\Gamma$ are, respectively, the tractions, electric displacements and magnetic inductions of the fundamental solutions given by Ding et al. (2005). Their superscripts $F$, $D$ and $B$ correspond to the solutions induced by point force, point electric charge and point electric current. $\|u_i\|$, $\|\varphi\|$ and $\|\psi\|$ are the displacement discontinuities, the electric potential discontinuity and the magnetic potential discontinuity across the crack faces, namely

$$\begin{aligned} \|u_i(\xi,\eta)\| &= u_i(\xi,\eta,h^+) - u_i(\xi,\eta,h^-), \\ \|\phi(\xi,\eta)\| &= \phi(\xi,\eta,h^+) - \phi(\xi,\eta,h^-), \quad i = 1,2,3, \\ \|\psi(\xi,\eta)\| &= \psi(\xi,\eta,h^+) - \psi(\xi,\eta,h^-), \end{aligned} \tag{7}$$

where superscripts "+" and "−" correspond to the physical quantities on the upper and lower crack faces, respectively.

Substituting the fundamental solutions in Ding et al. (2005) into Eq. (6), along with the kinematic Eq. (2) and constitutive Eq. (3), and further letting $h \to 0$, we obtain the extended stresses on the interface:

$$\begin{aligned} \sigma_{31}(x_1,x_2,0) = \int_{s^+}&\left\{\left[K_{11}(\xi-x_1)^2 + K_{12}(\eta-x_2)^2\right]\|u_1\| \right. \\ &\left. + (K_{11}-K_{12})(\xi-x_1)(\eta-x_2)\|u_2\|\right\} \\ &\times \frac{1}{\left[(\xi-x_1)^2+(\eta-x_2)^2\right]^{5/2}}dS + 2\pi K_{41}\frac{\partial\|u_3\|}{\partial x_1} \\ &+ 2\pi K_{42}\frac{\partial\|\varphi\|}{\partial x_1} + 2\pi K_{43}\frac{\partial\|\psi\|}{\partial x_1}, \end{aligned} \tag{8a}$$

$$\begin{aligned} \sigma_{32}(x_1,x_2,0) = \int_{s^+}&\left\{(K_{11}-K_{12})(\xi-x_1)(\eta-x_2)\|u_1\| + [K_{11}(\eta-x_2)^2 \right. \\ &\left. + K_{12}(\xi-x_1)^2]\|u_2\|\right\} \times \frac{1}{\left[(\xi-x_1)^2+(\eta-x_2)^2\right]^{5/2}}dS \\ &+ 2\pi K_{41}\frac{\partial\|u_3\|}{\partial x_2} + 2\pi K_{42}\frac{\partial\|\varphi\|}{\partial x_2} + 2\pi K_{43}\frac{\partial\|\psi\|}{\partial x_2}, \end{aligned} \tag{8b}$$

$$\begin{aligned} \sigma_{33}(x_1,x_2,0) = \int_{s^+}&[K_{z11}\|u_3\| + K_{z21}\|\varphi\| + K_{z31}\|\psi\|] \\ &\times \frac{1}{\left[(\xi-x_1)^2+(\eta-x_2)^2\right]^{3/2}}dS \\ &+ 2\pi K_1\left(\frac{\partial\|u_1\|}{\partial x_1} + \frac{\partial\|u_2\|}{\partial x_2}\right), \end{aligned} \tag{8c}$$

$$\begin{aligned} D_3(x_1,x_2,0) = \int_{s^+}&[K_{z12}\|u_3\| + K_{z22}\|\varphi\| + K_{z32}\|\psi\|] \\ &\times \frac{1}{\left[(\xi-x_1)^2+(\eta-x_2)^2\right]^{3/2}}dS + 2\pi K_2\left(\frac{\partial\|u_1\|}{\partial x_1} + \frac{\partial\|u_2\|}{\partial x_2}\right), \end{aligned} \tag{8d}$$

$$\begin{aligned} B_3(x_1,x_2,0) = \int_{s^+}&[K_{z13}\|u_3\| + K_{z23}\|\varphi\| + K_{z33}\|\psi\|] \\ &\times \frac{1}{\left[(\xi-x_1)^2+(\eta-x_2)^2\right]^{3/2}}dS + 2\pi K_3\left(\frac{\partial\|u_1\|}{\partial x_1} + \frac{\partial\|u_2\|}{\partial x_2}\right) \end{aligned} \tag{8e}$$

for the field points within the interfacial crack ($(x_1,x_2,0) \in S$), and

$$\begin{aligned} \sigma_{31}(x_1,x_2,0) = \int_{s^+}&\left\{\left[K_{11}(\xi-x_1)^2 + K_{12}(\eta-x_2)^2\right]\|u_1\| \right. \\ &\left. + (K_{11}-K_{12})(\xi-x_1)(\eta-x_2)\|u_2\|\right\} \\ &\times \frac{1}{\left[(\xi-x_1)^2+(\eta-x_2)^2\right]^{5/2}}dS, \end{aligned} \tag{9a}$$

$$\begin{aligned} \sigma_{32}(x_1,x_2,0) = \int_{s^+}&\left\{(K_{11}-K_{12})(\xi-x_1)(\eta-x_2)\|u_1\| \right. \\ &\left. + \left[K_{11}(\eta-x_2)^2 + K_{12}(\xi-x_1)^2\right]\|u_2\|\right\} \\ &\times \frac{1}{\left[(\xi-x_1)^2+(\eta-x_2)^2\right]^{5/2}}dS, \end{aligned} \tag{9b}$$

$$\begin{aligned} \sigma_{33}(x_1,x_2,0) = \int_{s^+}&[K_{z11}\|u_3\| + K_{z21}\|\varphi\| + K_{z31}\|\psi\|] \\ &\times \frac{1}{\left[(\xi-x_1)^2+(\eta-x_2)^2\right]^{3/2}}dS, \end{aligned} \tag{9c}$$

$$\begin{aligned} D_3(x_1,x_2,0) = \int_{s^+}&[K_{z12}\|u_3\| + K_{z22}\|\varphi\| + K_{z32}\|\psi\|] \\ &\times \frac{1}{\left[(\xi-x_1)^2+(\eta-x_2)^2\right]^{3/2}}dS, \end{aligned} \tag{9d}$$

$$\begin{aligned} B_3(x_1,x_2,0) = \int_{s^+}&[K_{z13}\|u_3\| + K_{z23}\|\varphi\| + K_{z33}\|\psi\|] \\ &\times \frac{1}{\left[(\xi-x_1)^2+(\eta-x_2)^2\right]^{3/2}}dS \end{aligned} \tag{9e}$$

for the field points outside the crack area ($(x_1, x_2, 0) \notin S$). The coefficients $K_{ij}$ and $K_{zij}$ in Eqs. (8) and (9) are material constants given in Appendix A (Zhao et al., 2008a).

Comparing Eqs. (8)-(9), it is observed that there are extra differential terms in Eq. (8) when the field point is located on the interfacial crack. It is these differential terms that make the coupling more complicated in bi-material systems. The interaction of two different material spaces through the interface may result in the lost of symmetry in interfacial crack behaviors. For example, a pure far-field tension may produce a combined stress field, i.e., the tensile and shear stress field, at the crack tip.

### 3.2. Green's functions of constant extended interfacial displacement discontinuities within a rectangular element

In practice, an arbitrarily shaped interfacial crack can be discretized into small constant rectangular elements, as shown in Fig. 2. If the integrals in Eqs. (8) and (9) over such an element can be calculated, the stresses at any field point can be obtained easily. Thus, in this subsection, we will derive the Green's functions due to constant extended interfacial displacement discontinuities within a rectangular element. For simplicity, we assume that the local coordinate system $(\xi, \eta)$ in Fig. 2 coincides with the global coordinate system $(x_1, x_2)$ on the interface and a general rectangular element with length of $2a$ and width of $2b$ is centered at the origin of the local coordinate system. Over the rectangular element, uniform extended displacement discontinuities with strengths of $\|u_i^e\|$ ($i = 1,2,3$), $\|\varphi^e\|$ and $\|\psi^e\|$ are distributed. Based on the definition of the Heaviside function, i.e.,

$$H(x) = \begin{cases} 1, & x \geqslant 0, \\ 0, & x < 0, \end{cases} \tag{10}$$

the extended displacement discontinuities within the constant rectangular element can be mathematically expressed as

$$\begin{aligned}
\|u_1(x_1,x_2)\| &= \|u_1^e\|(H(x_1+a) - H(x_1-a))(H(x_2+b) - H(x_2-b)), \\
\|u_2(x_1,x_2)\| &= \|u_2^e\|(H(x_1+a) - H(x_1-a))(H(x_2+b) - H(x_2-b)), \\
\|u_3(x_1,x_2)\| &= \|u_3^e\|(H(x_1+a) - H(x_1-a))(H(x_2+b) - H(x_2-b)), \\
\|\varphi(x_1,x_2)\| &= \|\varphi^e\|(H(x_1+a) - H(x_1-a))(H(x_2+b) - H(x_2-b)), \\
\|\psi(x_1,x_2)\| &= \|\psi^e\|(H(x_1+a) - H(x_1-a))(H(x_2+b) - H(x_2-b)).
\end{aligned} \tag{11}$$

Substituting Eq. (11) into Eqs. (8) and (9) and combining the obtained results inside and outside the element, we have finally the extended stresses at any point $(x_1, x_2, 0)$ on the interface:

$$\begin{aligned}
\sigma_{31}(x_1,x_2,0) = {} & [K_{11}I_1 + K_{12}I_2]\|u_1^e\| + (K_{11} - K_{12})I_3\|u_2^e\| \\
& + 2\pi\left(K_{41}\|u_3^e\| + K_{42}\|\varphi^e\| + K_{43}\|\psi^e\|\right) \times [\delta(x_1 \\
& + a) - \delta(x_1 - a)][H(x_2+b) - H(x_2-b)],
\end{aligned} \tag{12a}$$

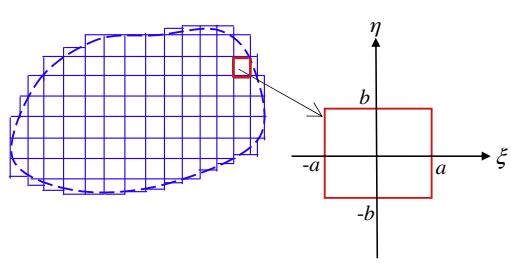


**Fig. 2.** Discretization of an arbitrary interfacial crack into $N$ rectangular elements.

$$\begin{aligned}
\sigma_{32}(x_1,x_2,0) = {} & (K_{11} - K_{12})I_3\|u_1^e\| + [K_{11}I_2 + K_{12}I_1]\|u_2^e\| \\
& + 2\pi\left(K_{41}\|u_3^e\| + K_{42}\|\varphi^e\| + K_{43}\|\psi^e\|\right) \\
& \times [H(x_1+a) - H(x_1-a)][\delta(x_2+b) - \delta(x_2-b)],
\end{aligned} \tag{12b}$$

$$\begin{aligned}
\sigma_{33}(x_1,x_2,0) = {} & \left(K_{z11}\|u_3^e\| + K_{z21}\|\varphi^e\| + K_{z31}\|\psi^e\|\right)(I_1 + I_2) \\
& + 2\pi K_1\{[\delta(x_1+a) - \delta(x_1-a)][H(x_2+b) \\
& - H(x_2-b)]\|u_1^e\| + [H(x_1+a) - H(x_1-a)][\delta(x_2+b) \\
& - \delta(x_2-b)]\|u_2^e\|\},
\end{aligned} \tag{12c}$$

$$\begin{aligned}
D_3(x_1,x_2,0) = {} & \left(K_{z12}\|u_3^e\| + K_{z22}\|\varphi^e\| + K_{z32}\|\psi^e\|\right)(I_1 + I_2) \\
& + 2\pi K_2\{[\delta(x_1+a) - \delta(x_1-a)][H(x_2+b) \\
& - H(x_2-b)]\|u_1^e\| + [H(x_1+a) - H(x_1-a)][\delta(x_2+b) \\
& - \delta(x_2-b)]\|u_2^e\|\},
\end{aligned} \tag{12d}$$

$$\begin{aligned}
B_3(x_1,x_2,0) = {} & \left(K_{z13}\|u_3^e\| + K_{z23}\|\varphi^e\| + K_{z33}\|\psi^e\|\right)(I_1 + I_2) \\
& + 2\pi K_3\{[\delta(x_1+a) - \delta(x_1-a)][H(x_2+b) \\
& - H(x_2-b)]\|u_1^e\| + [H(x_1+a) - H(x_1-a)][\delta(x_2+b) \\
& - \delta(x_2-b)]\|u_2^e\|\},
\end{aligned} \tag{12e}$$

where $\delta$ is the Dirac delta function, which is also defined as $\delta(x) = \mathrm{d}H(x)/\mathrm{d}x$; the three integrals $I_i$ ($i = 1,2,3$) are

$$\begin{aligned}
I_1(x_1,x_2,a,b) &= \int_{S_r} \frac{(\xi - x_1)^2}{\left[(\xi - x_1)^2 + (\eta - x_2)^2\right]^{5/2}} dS, \\
I_2(x_1,x_2,a,b) &= \int_{S_r} \frac{(\eta - x_2)^2}{\left[(\xi - x_1)^2 + (\eta - x_2)^2\right]^{5/2}} dS, \\
I_3(x_1,x_2,a,b) &= \int_{S_r} \frac{(\xi - x_1)(\eta - x_2)}{\left[(\xi - x_1)^2 + (\eta - x_2)^2\right]^{5/2}} dS,
\end{aligned} \tag{13}$$

where $S_r$ denotes the surface of the rectangular element. The three integrals in Eq. (13) over a general rectangular element as shown in Fig. 2 can be obtained analytically as below:

$$\begin{aligned}
I_1(x_1,x_2,a,b) = {} & -\frac{(x_1-a)^2 + 2(x_2-b)^2}{3(x_1-a)(x_2-b)\sqrt{(x_1-a)^2 + (x_2-b)^2}} \\
& + \frac{(x_1-a)^2 + 2(x_2+b)^2}{3(x_1-a)(x_2+b)\sqrt{(x_1-a)^2 + (x_2+b)^2}} \\
& + \frac{(x_1+a)^2 + 2(x_2-b)^2}{3(x_1+a)(x_2-b)\sqrt{(x_1+a)^2 + (x_2-b)^2}} \\
& - \frac{(x_1+a)^2 + 2(x_2+b)^2}{3(x_1+a)(x_2+b)\sqrt{(x_1+a)^2 + (x_2+b)^2}},
\end{aligned} \tag{14a}$$

$$\begin{aligned}
I_2(x_1,x_2,a,b) = {} & -\frac{2(x_1-a)^2 + (x_2-b)^2}{3(x_1-a)(x_2-b)\sqrt{(x_1-a)^2 + (x_2-b)^2}} \\
& + \frac{2(x_1-a)^2 + (x_2+b)^2}{3(x_1-a)(x_2+b)\sqrt{(x_1-a)^2 + (x_2+b)^2}} \\
& + \frac{2(x_1+a)^2 + (x_2-b)^2}{3(x_1+a)(x_2-b)\sqrt{(x_1+a)^2 + (x_2-b)^2}} \\
& - \frac{2(x_1+a)^2 + (x_2+b)^2}{3(x_1+a)(x_2+b)\sqrt{(x_1+a)^2 + (x_2+b)^2}},
\end{aligned} \tag{14b}$$

$$I_3(x_1,x_2,a,b) = \frac{1}{\sqrt{(x_1-a)^2+(x_2-b)^2}} - \frac{1}{\sqrt{(x_1-a)^2+(x_2+b)^2}} - \frac{1}{\sqrt{(x_1+a)^2+(x_2-b)^2}} + \frac{1}{\sqrt{(x_1+a)^2+(x_2+b)^2}}. \tag{14c}$$

It is observed from Eq. (13) that if the field point $(x_1,x_2)$ falls outside the integration area $S_r$, the three integrals in Eq. (13) are regular; If the integration area $S_r$ contains the field point $(x_1,x_2)$, the three integrals turn out to be divergent. However, the closed-form expressions in Eqs. (14a)–(14c) are proved to hold for both regular and divergent cases. We further point out that the obtained divergent integrals should be interpreted as finite-part integrals and that they can be found using the Hadamard regularization (Ioakimidis, 1982; Wang et al., 2001; Hadamard, 1923). The regularization procedure is briefly described below.

First, we introduce the polar coordinates as

$$\begin{aligned} \xi - x_1 &= r\cos\theta, \\ \eta - x_2 &= r\sin\theta. \end{aligned} \tag{15}$$

Thus, the general expression of the three integrals in Eq. (13) becomes

$$I = \mathcal{H}\int_\alpha^\beta \int_0^{R(\theta)} \frac{f(\theta)}{r^2} dr d\theta, \tag{16}$$

where $\mathcal{H}$ denotes the Hadamard finite-part integral; $f(\theta)$ is $\cos^2\theta$, $\sin^2\theta$ and $\cos\theta\sin\theta$ for $I_1$, $I_2$ and $I_3$, respectively.

We now assume that the divergent point $(\xi,\eta) = (x_1,x_2)$ is arbitrarily located within the rectangular area $\{\xi,\eta\} = \{(-a,a),(-b,b)\}$ as shown in Fig. 3. Then, the whole rectangular area is divided into eight triangular areas (Fig. 3). The integral in Eq. (16) is taken over each triangular area and the obtained results are added together to find the final integral expression. The integral in Eq. (16) has the singularity of order $r^{-2}$ and it can be evaluated in the Hadamard sense as

$$I = \mathcal{H}\int_\alpha^\beta f(\theta)\int_0^{R(\theta)} \frac{1}{r^2} dr d\theta = \int_\alpha^\beta \left[-\frac{f(\theta)}{R(\theta)}\right] d\theta. \tag{17}$$

Thus, the three divergent integrals can be evaluated by using Eq. (17) and the results turn out to be same as Eqs. (14a)–(14c). A detailed derivation for the divergent integral $I_1$ is given in Appendix B.

We define the extended stresses and extended displacements using the following notations

$$\sigma_{3I} = \begin{cases} \sigma_{3i} & I = i = 1,2,3, \\ D_3 & I = 4, \\ B_3 & I = 5, \end{cases} \qquad \|u_J^e\| = \begin{cases} \|u_j^e\| & J = j = 1,2,3, \\ \|\varphi^e\| & J = 4, \\ \|\psi^e\| & J = 5, \end{cases} \tag{18}$$

then the solutions in Eq. (12) can be expressed in a compact form as

$$\sigma_{3I}(x_1,x_2) = G_{IJ}^e(x_1,x_2)\|u_J^e\|, \tag{19}$$

where $G_{IJ}^e(x_1,x_2)$ are the Green's functions corresponding to the constant extended displacement discontinuities within the rectangular element of $\{x_1,x_2\} = \{\xi,\eta\} = \{(-a,a),(-b,b)\}$ on the interface. For instance, $G_{11}^e(x_1,x_2) = K_{11}I_1(x_1,x_2) + K_{12}I_2(x_1,x_2)$. The above Green's functions can be reduced to the solutions of the plane-strain interfacial crack problem by taking the limit of $b \to \infty$. Besides, the derived solutions can be reduced to those for the corresponding interfacial cracks in piezoelectric bi-materials by making the magnetic-related coefficients zero (Zhao et al., 2014).

### 3.3. Green's functions of point extended interfacial displacement discontinuities

In the last subsection, the Green's functions of constant extended interfacial displacement discontinuities within a rectangular element are obtained. When the size of the element approaches zero, i.e., $2a = 2b \to 0$, we can obtain the Green's functions or the fundamental solutions corresponding to the point extended interfacial displacement discontinuities, with the latter being defined as:

$$\begin{aligned} &\lim_{a\to 0} 4a^2\|u_1^p\| = 4a^2\|u_1^e\| = \|U\|, \\ &\lim_{a\to 0} 4a^2\|u_2^p\| = 4a^2\|u_2^e\| = \|V\|, \\ &\lim_{a\to 0} 4a^2\|u_3^p\| = 4a^2\|u_3^e\| = \|W\|, \\ &\lim_{a\to 0} 4a^2\|\varphi^p\| = 4a^2\|\varphi^e\| = \|\Phi\|, \\ &\lim_{a\to 0} 4a^2\|\psi^p\| = 4a^2\|\psi^e\| = \|\Psi\|, \end{aligned} \tag{20}$$

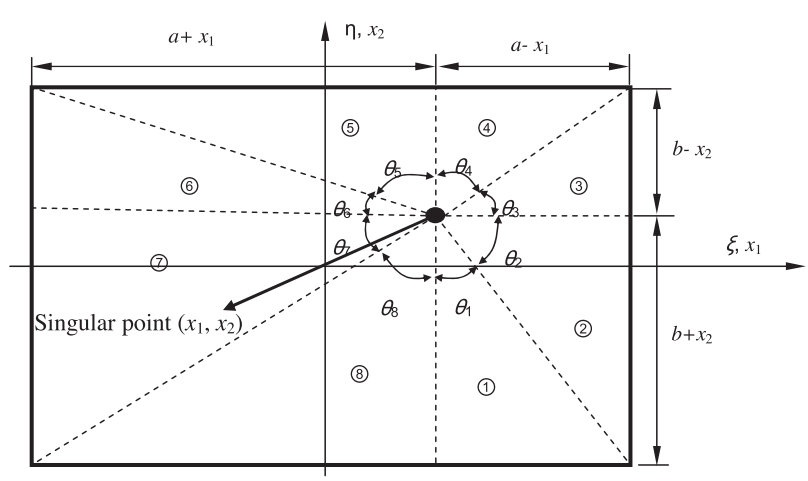


**Fig. 3.** Division of a rectangular integration area into eight triangular integration areas.

where $\|u_1\|$, $\|u_2\|$, $\|u_3\|$, $\|\varphi\|$ and $\|\psi\|$ with the superscript $p$ denote the point extended displacement discontinuities; $\|U\|$, $\|V\|$, $\|W\|$, $\|\Phi\|$ and $\|\Psi\|$ are the strength of the point extended displacement discontinuities. By this definition and based on the solutions in Section 3.2, the extended stresses at any point $(x_1,x_2,0)$ on the interface induced by the point extended interfacial displacement discontinuities can be expressed by

$$\begin{aligned}\sigma_{31}(x_1,x_2,0) = {} & [K_{11}J_1(x_1,x_2)+K_{12}J_2(x_1,x_2)]\|U\| \\ & + (K_{11}-K_{12})J_3(x_1,x_2)\|V\| \\ & + 2\pi(K_{41}\|W\|+K_{42}\|\Phi\|+K_{43}\|\Psi\|)\delta_{x_1}(x_1)\delta(x_2),\end{aligned} \tag{21a}$$

$$\begin{aligned}\sigma_{32}(x_1,x_2,0) = {} & (K_{11}-K_{12})J_3(x_1,x_2)\|U\| \\ & + [K_{11}J_2(x_1,x_2)+K_{12}J_1(x_1,x_2)]\|V\| \\ & + 2\pi(K_{41}\|W\|+K_{42}\|\Phi\|+K_{43}\|\Psi\|)\delta(x_1)\delta_{x_2}(x_2),\end{aligned} \tag{21b}$$

$$\begin{aligned}\sigma_{33}(x_1,x_2,0) = {} & (K_{z11}\|W\|+K_{z21}\|\Phi\|+K_{z31}\|\Psi\|)(J_1(x_1,x_2) \\ & + J_2(x_1,x_2)) \\ & + 2\pi K_1\{\delta_{x_1}(x_1)\delta(x_2)\|U\|+\delta(x_1)\delta_{x_2}(x_2)\|V\|\},\end{aligned} \tag{21c}$$

$$\begin{aligned}D_3(x_1,x_2,0) = {} & (K_{z12}\|W\|+K_{z22}\|\Phi\|+K_{z32}\|\Psi\|)(J_1(x_1,x_2)+J_2(x_1,x_2)) \\ & + 2\pi K_2\{\delta_{x_1}(x_1)\delta(x_2)\|U\|+\delta(x_1)\delta_{x_2}(x_2)\|V\|\},\end{aligned} \tag{21d}$$

$$\begin{aligned}B_3(x_1,x_2,0) = {} & (K_{z13}\|W\|+K_{z23}\|\Phi\|+K_{z33}\|\Psi\|)(J_1(x_1,x_2)+J_2(x_1,x_2)) \\ & + 2\pi K_3\{\delta_{x_1}(x_1)\delta(x_2)\|U\|+\delta(x_1)\delta_{x_2}(x_2)\|V\|\},\end{aligned} \tag{21e}$$

where $\delta_x(x)$ is the derivative of the Dirac delta function, i.e.,

$$\delta_x(x) = \frac{d\delta(x)}{dx}, \tag{22a}$$

and

$$\begin{aligned}J_1(x_1,x_2) &= \lim_{a\to 0}\frac{I_1(x_1,x_2,a)}{4a^2} = \frac{x_1^2}{(x_1^2+x_2^2)^{5/2}}, \\ J_2(x_1,x_2) &= \lim_{a\to 0}\frac{I_2(x_1,x_2,a)}{4a^2} = \frac{x_2^2}{(x_1^2+x_2^2)^{5/2}}, \\ J_3(x_1,x_2) &= \lim_{a\to 0}\frac{I_3(x_1,x_2,a)}{4a^2} = \frac{x_1x_2}{(x_1^2+x_2^2)^{5/2}}.\end{aligned} \tag{22b}$$

Again, by making use of the compact notations in Eq. (18), solutions in Eq. (21) can be rewritten as

$$\sigma_{3I}(x_1,x_2) = G_{IJ}^p(x_1,x_2)\|u_J^p\|, \tag{23}$$

where $G_{IJ}^p(x_1,x_2)$ denotes the Green's functions for the point extended interfacial displacement discontinuities applied at $(x_1,x_2) = (0,0)$. For example, $G_{11}^p(x_1,x_2) = K_{11}J_1(x_1,x_2)+K_{12}J_2(x_1,x_2)$.

The application of constant displacement discontinuities may be relatively limited, but the obtained point Green's functions are very flexible in solving interfacial crack problems with complex boundary conditions and geometries. Furthermore, the higher order elements, e.g., linear or quadratic elements, can be constructed simply by integrating the Green's function of the point extended interfacial displacement discontinuities.

## 4. Extended stress intensity factors and energy release rate

### 4.1. Approximations of Dirac delta and Heaviside functions

We point out that the solutions containing the Dirac delta function will cause oscillating singularity in the extended stresses (Zhao et al., 2014). Therefore, before performing fracture analysis, the Dirac delta function in the solutions is approximated by the Gaussian distribution function as

$$\delta(x) = \frac{1}{\sqrt{2\pi}\varepsilon}\exp\left[-\frac{x^2}{2\varepsilon^2}\right], \tag{24}$$

where $0 < \varepsilon < 1$. The selection and the effect of the parameter $\varepsilon$ on the fracture parameters will be discussed later in the numerical analysis section.

Correspondingly, the derivative of the Dirac delta function is given by

$$\delta_x(x) = \frac{d\delta(x)}{dx} = -\frac{x}{\sqrt{2\pi}\varepsilon^3}\exp\left[-\frac{x^2}{2\varepsilon^2}\right]. \tag{25}$$

On the other hand, as we know, the Heaviside function is the integral of the Dirac delta function. Thus, if the Dirac delta function is given by Eq. (24), the Heaviside function should be determined by

$$\begin{aligned}H(x) &= \int_{-\infty}^{x}\frac{1}{\sqrt{2\pi}\varepsilon}\exp\left[-\frac{y^2}{2\varepsilon^2}\right]dy = \frac{1}{\sqrt{\pi}}\int_{-\infty}^{x/(\sqrt{2}\varepsilon)}\exp\left[-t^2\right]dt \\ &= \frac{1}{2}\left(1+\mathrm{Erf}\left[\frac{x}{\sqrt{2}\varepsilon}\right]\right),\end{aligned} \tag{26}$$

where Erf is the integral of the Gaussian distribution or the Error function.

### 4.2. Extended stress intensity factors and energy release rate

For simplicity, a local coordinate system $(\beta_1,\beta_2,\beta_3)$ is introduced so that its origin $p$ coincides with a point on the crack front of interest (Fig. 4). The $\beta_1$-axis is perpendicular to the crack front line and directs towards the inner side of the crack, while the $\beta_2$-axis is tangential to the crack front line, and $\beta_3$ is parallel to the global $x_3$-axis. Now we consider the point $(\beta_1,\beta_2,\beta_3) = (-\rho,0,0)$ $(\rho > 0)$ outside the crack but close to the point $p$. By introducing the transformation

$$(\xi+\rho) = r\cos\theta, \quad \eta = r\sin\theta, \tag{27}$$

the extended stresses in Eq. (9) at point $(-\rho,0,0)$ become

$$\begin{aligned}\sigma_{31}(-\rho,0,0) = \int_{s^+}\Big\{ & \left[K_{11}\cos^2\theta+K_{12}\sin^2\theta\right]\|u_1\| \\ & + (K_{11}-K_{12})\cos\theta\sin\theta\|u_2\|\Big\}\frac{1}{r^3}dS,\end{aligned} \tag{28a}$$

$$\begin{aligned}\sigma_{32}(-\rho,0,0) = \int_{s^+}\{ & (K_{11}-K_{12})\cos\theta\sin\theta\|u_1\| \\ & + \left[K_{11}\sin^2\theta+K_{12}\cos^2\theta\right]\|u_2\|\Big\}\frac{1}{r^3}dS,\end{aligned} \tag{28b}$$

$$\sigma_{33}(-\rho,0,0) = \int_{s^+}[K_{z11}\|u_3\|+K_{z21}\|\varphi\|+K_{z31}\|\psi\|]\frac{1}{r^3}dS, \tag{28c}$$

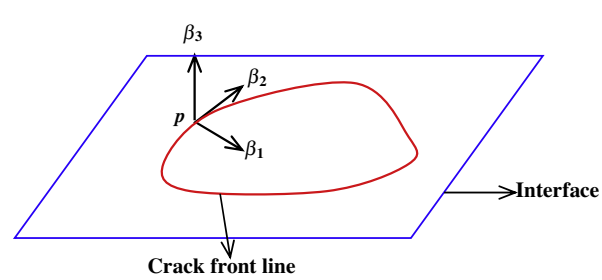


**Fig. 4.** Local coordinate system $(\beta_1,\beta_2,\beta_3)$ at a point $p$ on the front line of the interfacial crack.

$$D_3(-\rho,0,0)=\int_{s^+}[K_{z12}\|u_3\|+K_{z22}\|\varphi\|+K_{z32}\|\psi\|]\frac{1}{r^3}dS, \tag{28d}$$

$$B_3(-\rho,0,0)=\int_{s^+}[K_{z13}\|u_3\|+K_{z23}\|\varphi\|+K_{z33}\|\psi\|]\frac{1}{r^3}dS. \tag{28e}$$

Thus, the extended stress intensity factors at the crack front can be defined as

$$\begin{aligned}
K_{\mathrm{I}}^F&=\lim_{\rho\to0}\sqrt{2\pi\rho}\sigma_{33}(-\rho,0,0),\\
K_{\mathrm{I}}^D&=\lim_{\rho\to0}\sqrt{2\pi\rho}D_3(-\rho,0,0),\\
K_{\mathrm{I}}^B&=\lim_{\rho\to0}\sqrt{2\pi\rho}B_3(-\rho,0,0),\\
K_{\mathrm{II}}^F&=\lim_{\rho\to0}\sqrt{2\pi\rho}\sigma_{31}(-\rho,0,0),\\
K_{\mathrm{III}}^F&=\lim_{\rho\to0}\sqrt{2\pi\rho}\sigma_{32}(-\rho,0,0),
\end{aligned} \tag{29}$$

where $K$ with the superscripts F, D and B denote, respectively, the stress intensity factors, the electric displacement intensity factor and the magnetic induction intensity factor.

We point out that Eqs. (28a)–(28e) are similar to the corresponding ones for the homogeneous transversely isotropic MEE materials in Zhao et al. (2007), except that the coefficients $K_{ij}$ and $K_{zij}$ in the integrals are different in both cases and that the oscillatory singularity is removed due to the replacement of the Dirac delta function by the Gaussian distribution function. Therefore, the extended stresses at the crack front only possess the ordinary singularity of order $r^{-1/2}$. The singularity of the stresses at the four corners of a rectangular crack is quite complicated, but with an order of singularity below 1/2 (Schmitz et al., 1993; Cruse, 1996). As important fracture parameters, we now derive the formulas for the extended stress intensity factors and $J$-integral. By following the approach in Zhao et al. (2007), the extended stress intensity factors at the crack front can be expressed as:

$$\begin{aligned}
K_{\mathrm{I}}^F&=\sqrt{2\pi}\pi\lim_{\rho\to0}[K_{z11}\|u_3\|+K_{z21}\|\varphi\|+K_{z31}\|\psi\|]/\sqrt{\rho},\\
K_{\mathrm{I}}^D&=\sqrt{2\pi}\pi\lim_{\rho\to0}[K_{z12}\|u_3\|+K_{z22}\|\varphi\|+K_{z32}\|\psi\|]/\sqrt{\rho},\\
K_{\mathrm{I}}^B&=\sqrt{2\pi}\pi\lim_{\rho\to0}[K_{z13}\|u_3\|+K_{z23}\|\varphi\|+K_{z33}\|\psi\|]/\sqrt{\rho},\\
K_{\mathrm{II}}^F&=\frac{\sqrt{2\pi}\pi}{3}\lim_{\rho\to0}[2K_{11}+K_{12}]\|u_1\|/\sqrt{\rho},\\
K_{\mathrm{III}}^F&=\frac{\sqrt{2\pi}\pi}{3}\lim_{\rho\to0}[K_{11}+2K_{12}]\|u_2\|/\sqrt{\rho}.
\end{aligned} \tag{30}$$

The $J$-integral is given by Beom and Atluri (1996) and Zhang et al. (2002)

$$J=\frac{1}{4}\mathbf{K}^T\mathbf{H}\mathbf{K}, \tag{31}$$

where $\mathbf{K}=\left(K_{\mathrm{II}}^F\quad K_{\mathrm{I}}^F\quad K_{\mathrm{III}}^F\quad K_{\mathrm{I}}^D\quad K_{\mathrm{I}}^B\right)^{\mathrm{T}}$ is the vector of the extended stress intensity factors and

$$\begin{aligned}
\mathbf{H}&=\left[\mathrm{Re}\left(\mathbf{Y}^+ + \mathbf{Y}^-\right)\right]\left(\mathbf{I}+\mathbf{M}^2\right)=(\mathbf{I}+i\mathbf{M})^T\left[\mathrm{Re}\left(\mathbf{Y}^+ + \mathbf{Y}^-\right)\right](\mathbf{I}+i\mathbf{M}),\\
\mathbf{M}&=-\left[\mathrm{Re}\left(\mathbf{Y}^+ + \mathbf{Y}^-\right)\right]^{-1}\left[\mathrm{Im}\left(\mathbf{Y}^+ - \mathbf{Y}^-\right)\right],
\end{aligned} \tag{32}$$

where matrix $\mathbf{Y}$ is defined in Appendix C and its superscripts "+" and "−" correspond to the upper and the lower material spaces, respectively.

## 5. Extended displacement discontinuity method

Crouch (1976) first introduced the displacement discontinuity method. He placed $N$ displacement discontinuities of unknown magnitude along the boundaries of the region to be analyzed. A system of algebraic equations is then formed and solved for the discontinuity values that produce the prescribed boundary tractions or displacements. This method will be extended in the present study to analyze the rectangular interfacial crack in 3D MEE bimaterials.

Although the interfacial crack can be of arbitrary shape, only rectangular cracks are assumed as illustration in the numerical study. We assume that a rectangular interfacial crack is divided into $N = N_1 \times N_2$ elements as in Section 3.2. Constant extended displacement discontinuities of unknown magnitudes are distributed within each element. The influence functions which are essential in the extended Crouch's method have been obtained as the Green's functions in Section 3.2. It should be noted that solutions in Eq. (12) are derived in local coordinate system. Thus, in global system, it follows that the stress $\sigma_{3l}^k$ at the centre of the $k$th element due to the extended displacement discontinuities $\|u_j^{e_l}\|$ within the $l$th constant element is

$$\sigma_{3l}^k(x_{1k},x_{2k};x_{1l},x_{2l})=G_{Ij}^{e_l}(x_{1k}-x_{1l},x_{2k}-x_{2l})\|u_j^{e_l}\|, \tag{33}$$

where $(x_{1k},x_{2k})$ and $(x_{1l},x_{2l})$ define the positions of the element centers, and relative coordinates $(x_{ik}–x_{il})$ are used. By superposition, the total extended stresses at the centre of the $k$th element due to extended displacement discontinuities in all $N$ elements is simply

$$\sigma_{3l}^k(x_{1k},x_{2k})=\sum_{l=1}^{N}G_{Ij}^{e_l}(x_{1k}-x_{1l},x_{2k}-x_{2l})\|u_j^{e_l}\|. \tag{34}$$

Then the solution of the prescribed interfacial crack problem is specified by the solution of a system of $5N$ linear equations with $5N$ unknowns:

$$t_I^0 f(x_{1k},x_{2k})=\sum_{l=1}^{N}G_{Ij}^{e_l}(x_{1k}-x_{1l},x_{2k}-x_{2l})\|u_j^{e_l}\|, \tag{35}$$

where $f(x_1,x_2)$ on the left side is the distribution function of the loadings prescribed on the crack faces and $t^0$ is the loading strength. It can be seen that the prescribed extended tractions are not necessarily uniform along the whole crack faces and if they are uniformly distributed then $f(x_1,x_2)\equiv 1$. It should be pointed out that if the discontinuities are distributed symmetrically about the centre of the crack, Eq. (35) can be reduced to a $5N/2$ by $5N/2$ system of equations.

The extended displacement discontinuities close to the crack tip can be extrapolated by fitting the calculated results of the elements at the front of it and the fitting equations are shown as below:

$$\|u_J\|=\chi_{J1}r^{1/2}+\chi_{J2}r^{3/2},\quad J=1,2,3,4,5, \tag{36}$$

where $\chi_{J1}$ and $\chi_{J2}$ are fitting coefficients and $r$ here denotes the distance of the field point from the crack tip. Then by substituting Eq. (36) into Eq. (30), the extended stress intensity factors become

$$\begin{aligned}
K_{\mathrm{I}}^F&=\sqrt{2\pi}\pi(K_{z11}\chi_{31}+K_{z21}\chi_{41}+K_{z31}\chi_{51}),\\
K_{\mathrm{I}}^D&=\sqrt{2\pi}\pi(K_{z12}\chi_{31}+K_{z22}\chi_{41}+K_{z32}\chi_{51}),\\
K_{\mathrm{I}}^B&=\sqrt{2\pi}\pi(K_{z13}\chi_{31}+K_{z23}\chi_{41}+K_{z33}\chi_{51}),\\
K_{\mathrm{II}}^F&=\frac{\sqrt{2\pi}\pi}{3}(2K_{11}+K_{12})\chi_{11},\\
K_{\mathrm{III}}^F&=\frac{\sqrt{2\pi}\pi}{3}(K_{11}+2K_{12})\chi_{21}.
\end{aligned} \tag{37}$$

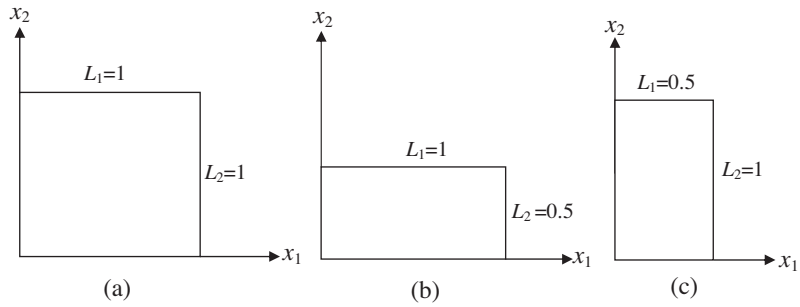


**Fig. 5.** Three different sizes of the rectangular interfacial crack.

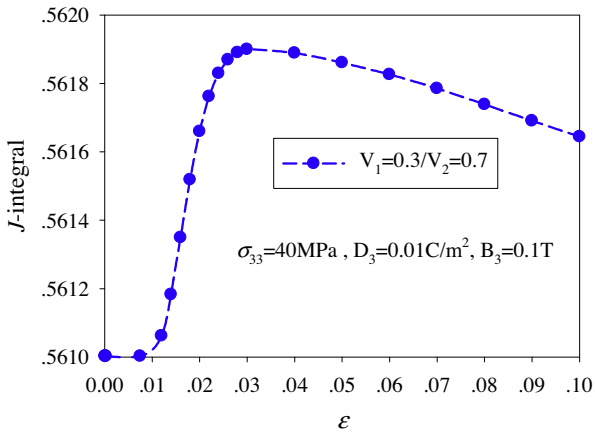


**Fig. 6a.** Variation of the maximum dimensionless $J$-integral along the edge of the square interfacial crack with different $\varepsilon$ values under $\sigma_{33}$ = 40 MPa, $D_3$ = 0.01 C/m$^2$ and $B_3$ = 0.1 T for the material system of $V_1$ = 0.3/$V_2$ = 0.7.

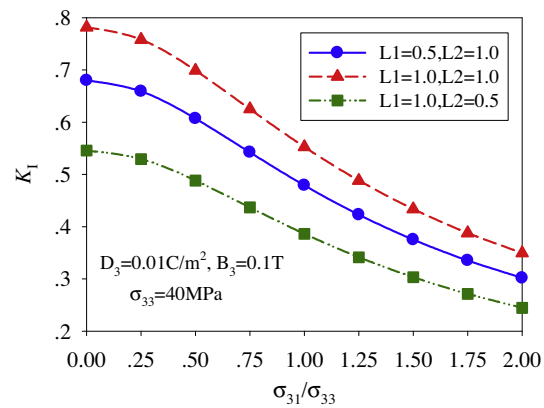


**Fig. 7a.** Variation of the maximum dimensionless stress intensity factor $K_I$ on the edge of $x_1$ = 0 of the rectangular interfacial crack with different applied stress ratios of $\sigma_{31}/\sigma_{33}$, three different crack sizes are considered.

## 6. Numerical examples

In the following numerical examples, the piezoelectric material $BaTiO_3$ and the piezomagnetic material $CoFe_2O_4$ are used to compose the MEE composite. The available material constants of these two constituents are listed in Appendix D. If $m_1$–$m_2$–$m_3$ denotes the material coordinate system, then the poling direction of the given materials in Appendix D is along the $m_3$-direction. The material constants of the resultant MEE composite can be obtained by following the rule of mixture:

$$\Lambda^c = \Lambda^e V_i + \Lambda^m (1 - V_i), \tag{38}$$

where $V_i$ is the volume fraction of the piezoelectric component $BaTiO_3$ ($i$ = 1, 2 are for the upper and lower material spaces, respectively); $\Lambda$ with the superscripts "$c$", "$e$" and "$m$" denote, respectively, the material constants of the composite, the piezoelectric component $BaTiO_3$ and the piezomagnetic component $CoFe_2O_4$. In the following numerical examples, the material coordinate system

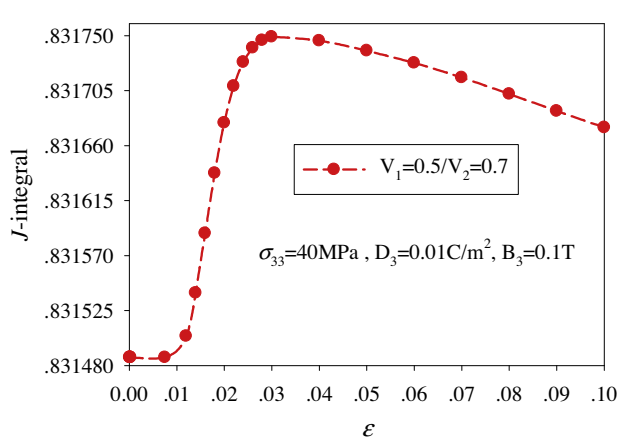


**Fig. 6b.** Variation of the maximum dimensionless $J$-integral along the edge of the square interfacial crack with different $\varepsilon$ values under $\sigma_{33}$ = 40 MPa, $D_3$ = 0.01 C/m$^2$ and $B_3$ = 0.1 T for the material system of $V_1$ = 0.5/$V_2$ = 0.7.

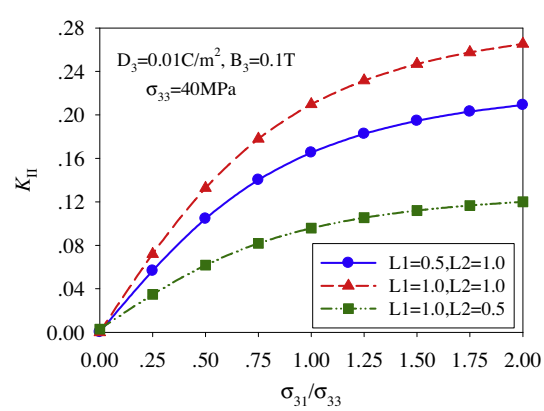


**Fig. 7b.** Variation of the maximum dimensionless stress intensity factor $K_{II}$ on the edge of $x_1$ = 0 of the rectangular interfacial crack with different applied stress ratios of $\sigma_{31}/\sigma_{33}$, three different crack sizes are considered.

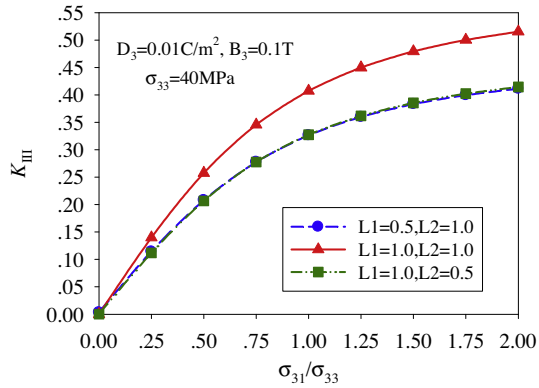


**Fig. 7c.** Variation of the maximum dimensionless stress intensity factor $K_{III}$ on the edge of $x_1 = 0$ of the rectangular interfacial crack with different applied stress ratios of $\sigma_{31}/\sigma_{33}$, three different crack sizes are considered.

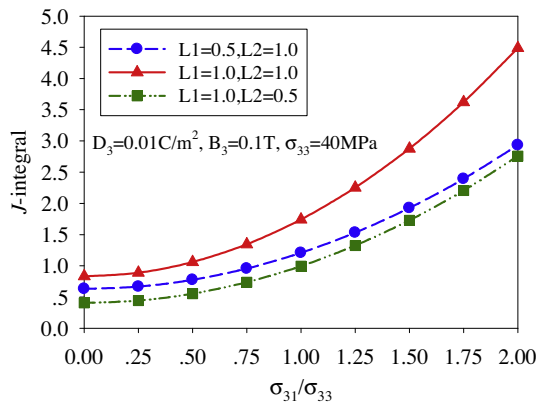


**Fig. 7d.** Variation of the maximum dimensionless $J$-integral on the edge of $x_1 = 0$ of the rectangular interfacial crack with different applied stress ratios of $\sigma_{31}/\sigma_{33}$, three different crack sizes are considered.

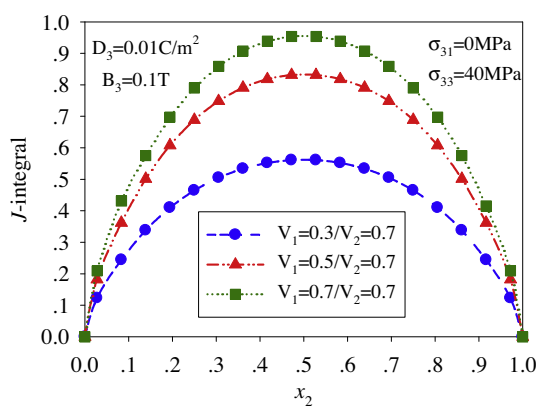


**Fig. 8a.** Distribution of the dimensionless $J$-integral along the edge of $x_1 = 0$ of the square interfacial crack under $\sigma_{33} = 40$ MPa, $D_3 = 0.01$ C/m$^2$ and $B_3 = 0.1$ T and $\sigma_{31} = 0$ MPa, three different bi-material systems are considered.

$m_1$–$m_2$–$m_3$ of the obtained transversely isotropic composite is made to coincide with the global coordinate system $x_1$–$x_2$–$x_3$. Three different crack sizes will be considered for the rectangular interfacial crack as shown in Fig. 5 ((a)–(c)). It should be noted that all the geometric quantities and the obtained displacement discontinuities in the numerical examples are normalized by length $l = 1$ m. The stress

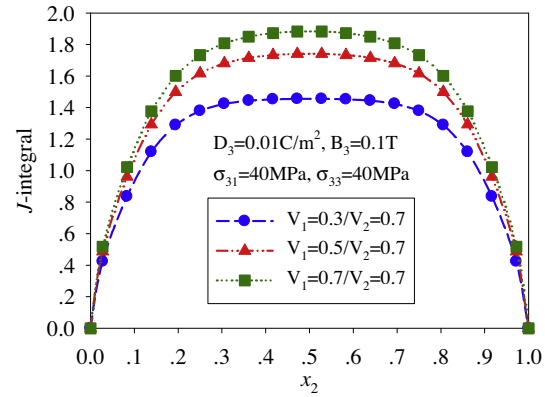


**Fig. 8b.** Distribution of the dimensionless $J$-integral along the edge of $x_1 = 0$ of the square interfacial crack under $\sigma_{33} = 40$ MPa, $D_3 = 0.01$ C/m$^2$ and $B_3 = 0.1$ T and $\sigma_{31} = 40$ MPa, three different bi-material systems are considered.

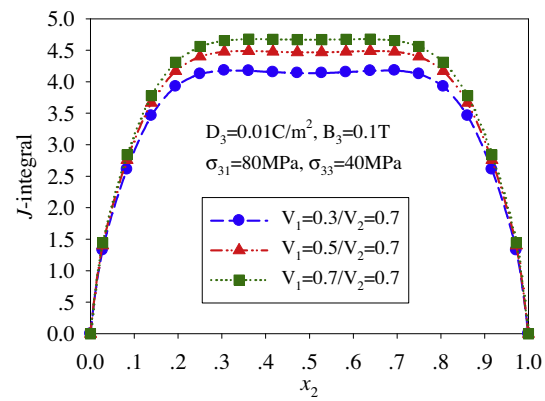


**Fig. 8c.** Distribution of the dimensionless $J$-integral along the edge of $x_1 = 0$ of the square interfacial crack under $\sigma_{33} = 40$ MPa, $D_3 = 0.01$ C/m$^2$ and $B_3 = 0.1$ T and $\sigma_{31} = 80$ MPa, three different bi-material systems are considered.

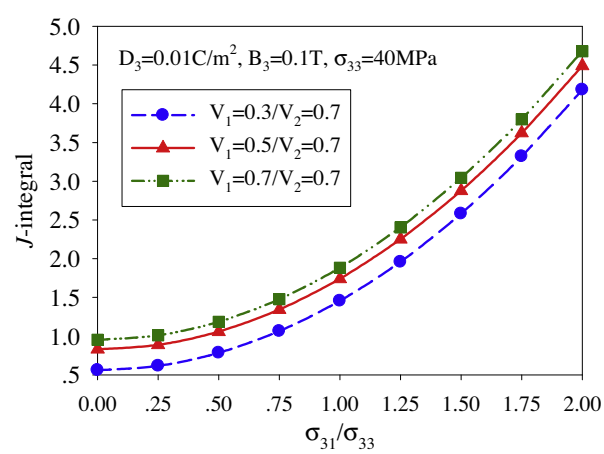


**Fig. 9.** Variation of the maximum dimensionless $J$-integral on the edge of $x_1 = 0$ of the square interfacial crack with different applied stress ratios of $\sigma_{31}/\sigma_{33}$, three different bi-material systems are considered.

intensity factors $K$ ($K_I$, $K_{II}$ and $K_{III}$) are normalized by $\sqrt{\pi l/2}\sigma_e$, where $\sigma_e$ is the effective stress which is defined differently for specific cases. The electric displacement intensity factor $K_D$ and the magnetic induction intensity factor $K_B$ are normalized by $\sqrt{\pi l/2}D_3$

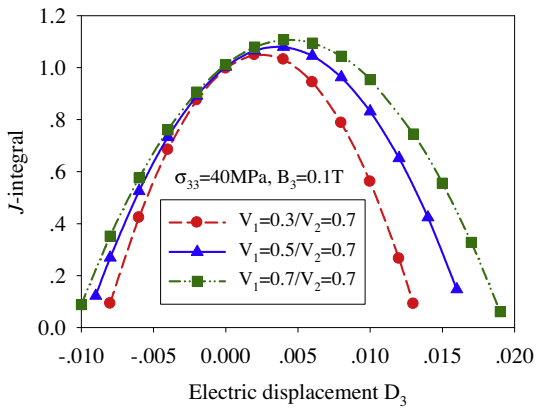


**Fig. 10.** Variation of the maximum dimensionless $J$-integral on the edge of $x_1 = 0$ of the square interfacial crack with different applied electric displacement $D_3$, three different bi-material systems are considered.

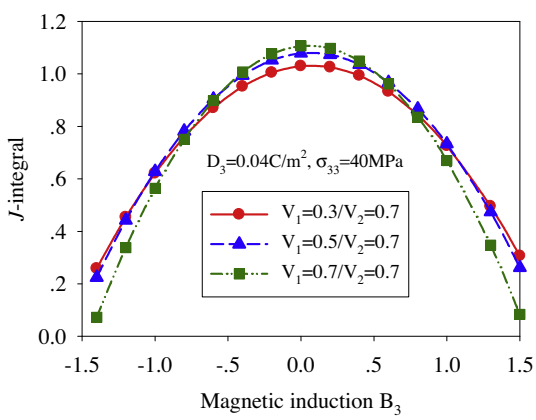


**Fig. 11.** Variation of the maximum dimensionless $J$-integral on the edge of $x_1 = 0$ of the square interfacial crack with different applied magnetic induction $B_3$, three different bi-material systems are considered.

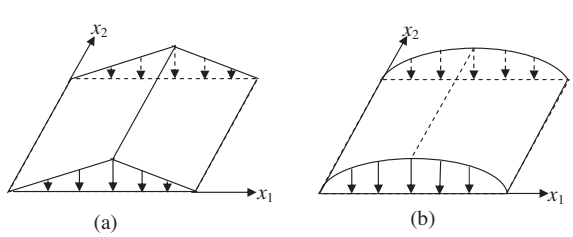


**Fig. 12.** Loadings of (a) linear distribution and (b) parabolic distribution on the crack face.

and $\sqrt{\pi l/2}B_3$, respectively, with $D_3$ being the applied electric displacement and $B_3$ the applied magnetic induction. The energy release rate $J$-integral is always normalized by $c_{33}/(l\sigma_{33}^2)$, with $\sigma_{33}$ being the applied traction component and $c_{33}$ the elastic constant of $BaTiO_3$.

As mentioned in Section 3.2, our solutions can be reduced to the ones for the plane-strain interfacial cracks in piezoelectric bi-materials as in Zhao et al. (2014). Furthermore, our solutions can be reduced to the ones for cracks in 3D homogeneous MEE full space as in Zhao et al. (2007). We have numerically checked our

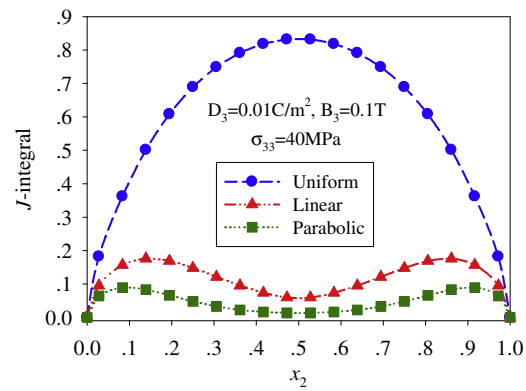


**Fig. 13a.** Variation of the dimensionless $J$-integral along the edge of $x_2 = 0$ of the square interfacial crack under loadings, respectively, of uniform, linear and parabolic distribution.

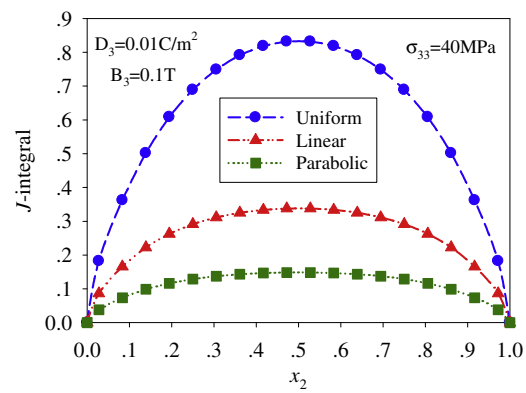


**Fig. 13b.** Variation of the dimensionless $J$-integral along the edge of $x_1 = 0$ of the square interfacial crack under loadings, respectively, of uniform, linear and parabolic distribution.

formulations for these reduced cases and found that our solutions are correct.

As mentioned in Section 4.1, the parameter $\varepsilon$ in Eqs. (24) and (25) should be assigned properly. Thus, numerical study on the effect of different values of the parameter $\varepsilon$ on the $J$-integral is necessary. Fig. 6 shows the variation of the maximum dimensionless $J$-integral along the edge of the square-shaped interfacial crack (as shown in Fig. 5a) with different $\varepsilon$ values under the loading of $\sigma_{33} = 40$ MPa, $D_3 = 0.01$ C/m$^2$ and $B_3 = 0.1$ T for volume fractions of $V_1 = 0.3/V_2 = 0.7$ (Fig. 6a) and $V_1 = 0.5/V_2 = 0.7$ (Fig. 6b). From Fig. 6, it can be seen that as $\varepsilon$ approaches zero, $J$-integral approaches a constant value which is the minimum value of $J$; when $\varepsilon$ is near the value of 0.03, $J$-integral has a maximum value. However, the difference between them is far less than 1% and can be consequently neglected. Furthermore, similar results are obtained for different rectangular-shaped cracks and for different material volume fractions. As such, in the following calculations, we assume $\varepsilon = 0.0075$.

Figs. 7a–7c show, respectively, the variations of the maximum dimensionless stress intensity factors $K_I$, $K_{II}$ and $K_{III}$ on the left edge ($x_1 = 0$) of the rectangular interfacial crack with different applied stress ratio $\sigma_{31}/\sigma_{33}$ for which the value of $\sigma_{33}$ is fixed at 40 MPa. The electric displacement of $D_3 = 0.01$ C/m$^2$ and the magnetic induction of $B_3 = 0.1$ T are also applied. The effective stress to normalize the stress intensity factors here is calculated as $\sigma_e = \sqrt{\sigma_{31}^2 + \sigma_{33}^2}$. In all the following calculations, unless mentioned specifically such as Fig. 9, the volume fractions of the

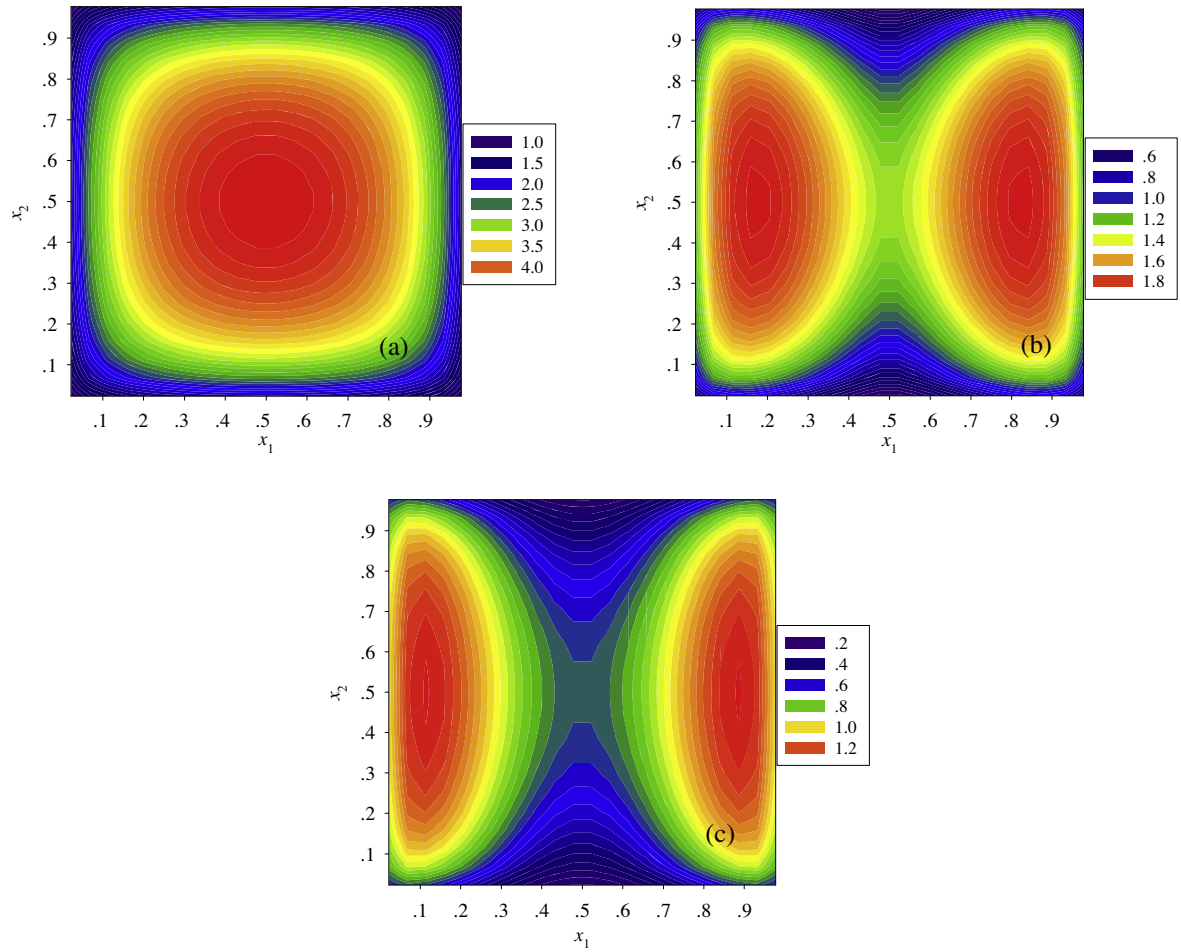


**Fig. 14.** Dimensionless displacement discontinuity $\|u_3\|$ ($\times 10^{-4}$) on the whole square interfacial crack under mixed loadings of (a) uniform distribution; (b) linear distribution; and (c) parabolic distribution.

piezoelectric constituent for the upper and the lower material spaces are $V_1 = 0.5$ and $V_2 = 0.7$, respectively. From Fig. 7, it can be seen that the normal stress intensity factor $K_I$ (Fig. 7a) decreases, whilst both shear stress intensity factors $K_{II}$ (Fig. 7b) and $K_{III}$ (Fig. 7c) increase with the increasing ratio of $\sigma_{31}/\sigma_{33}$. It is observed that nonzero $K_{III}$ occurs even though no $\sigma_{32}$ is applied. This demonstrates the special coupling relation mentioned in Section 3.1. Meanwhile, we found that the maximum values of these three stress intensity factors all occur at the middle of the crack edge. Besides, the electric displacement intensity factor $K_D$ and the magnetic induction intensity factor $K_B$ also change with applied shear stresses. However, their changes are little as compared to the stress intensity factors so that their differences are neglected. Fig. 7d shows the variation of the maximum dimensionless energy release rate $J$-integral on the left crack edge ($x_1 = 0$) with different ratios of $\sigma_{31}/\sigma_{33}$ for different crack shapes. It is found that the maximum $J$-integral does not always occur at the center of the crack edge and its location is affected by the applied shear loadings, which can be seen in the following part.

Fig. 8 shows the distribution of the dimensionless $J$-integral along the left edge ($x_1 = 0$) of the square interfacial crack (Fig. 5a) under $\sigma_{33} = 40$ MPa, $D_3 = 0.01$ C/m$^2$ and $B_3 = 0.1$ T with $\sigma_{31} = 0$ MPa, 40 MPa and 80 MPa in Figs. 8a, 8b and 8c, respectively. Different volume fractions of the piezoelectric $BaTiO_3$, namely $V_1 = 0.3$, $V_1 = 0.5$, and $V_1 = 0.7$ are considered for the upper material space, whilst the volume faction for the lower material space remains $V_2 = 0.7$. In Figs. 8a and 8b, the maximum $J$-integral is located at the center of the left crack edge. However, in Fig. 8c, maximum $J$-integral is located symmetrically on two sides of the edge center. Besides, the $J$-integral at corners of the rectangular crack are zero as shown in Figs. 8a–8c. Actually, as mentioned in Section 4.2, the singularity at four corners of a rectangular crack is weak, and thus the stress intensity factors at four corners is zero, which was also reported in Pan and Yuan (2000), Wang et al. (2001) and Noda and Kihara (2002) for rectangular cracks in elastic material. It also can be seen that the $J$-integral of the homogeneous case is larger than that of the bi-material cases. In other words, the interface between the two material spaces implements a stronger restriction on the crack propagation under the current loading case if $J$-integral is adopted as the fracture criteria.

Fig. 9 shows the variation of the maximum dimensionless $J$-integral on the left edge ($x_1 = 0$) of the square interfacial crack with different ratios of $\sigma_{31}/\sigma_{33}$ for three different bi-material systems. Again, $\sigma_{33}$ is fixed at 40 MPa, and $D_3 = 0.01$ C/m$^2$ and $B_3 = 0.1$ T are also applied. Figs. 10 and 11 present, respectively, the effect of different electric loading and the effect of different magnetic loading on the maximum dimensionless $J$-integral on the left edge ($x_1 = 0$) of the square interfacial crack. Fig. 10 indicates that there exists a critical value of the applied electric displacement for each bi-material system which induces the maximum $J$-integral. The $J$-integral decreases monotonically and symmetrically towards zero on two sides of this critical value. This critical value of the applied electric displacement for material systems $V_1 = 0.3/V_2 = 0.7$, $V_1 = 0.5/V_2 = 0.7$ and $V_1 = 0.7/V_2 = 0.7$ is approximately 0.0025 C/m$^2$, 0.004 C/m$^2$ and 0.005 C/m$^2$, respectively. Similarly, as shown in Fig. 11, there also exists a critical value of the applied magnetic

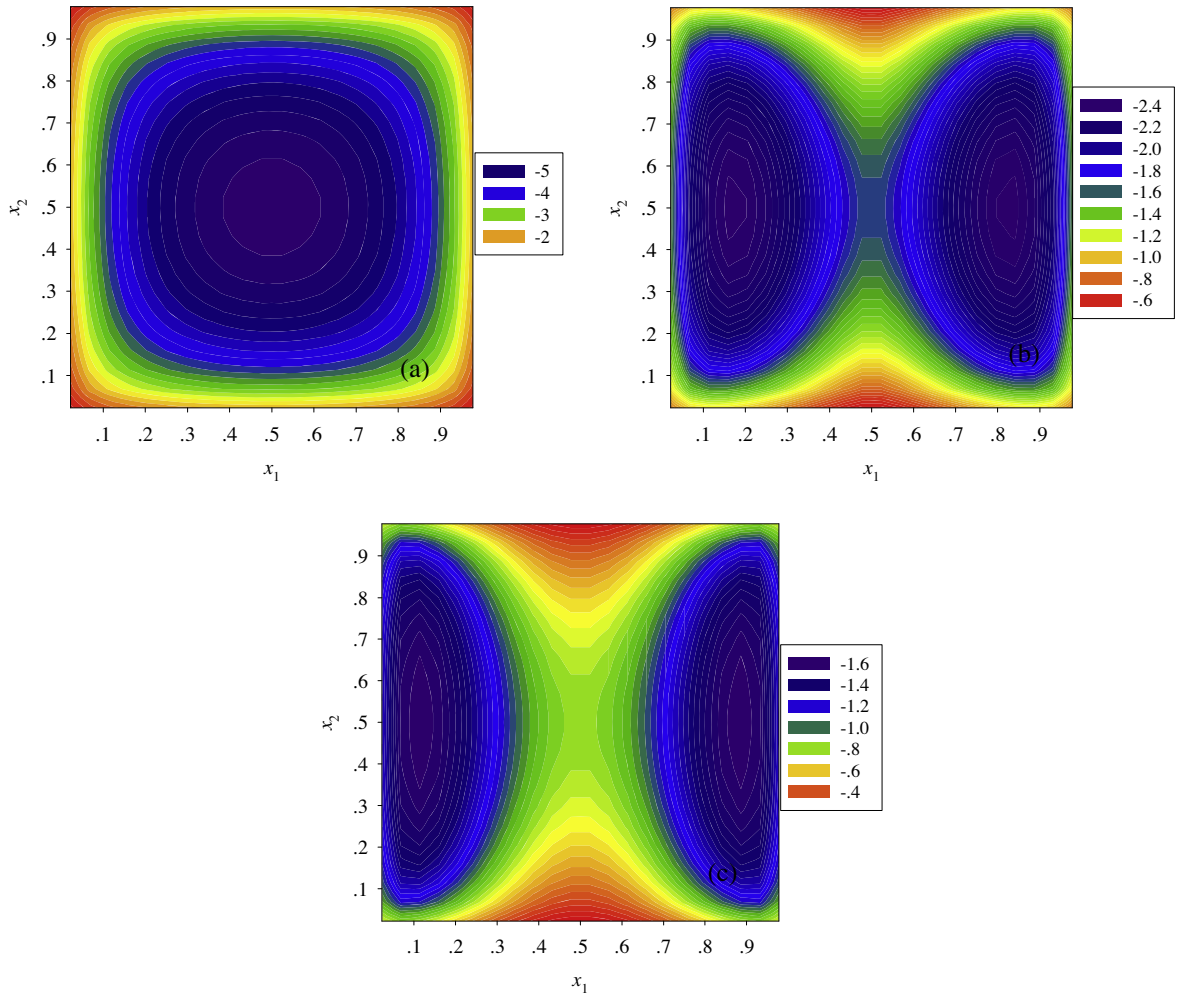


**Fig. 15.** Dimensionless electric potential jump $||\varphi||$ ($\times 10^{-4}$) on the whole square interfacial crack under mixed loadings of (a) uniform distribution; (b) linear distribution; and (c) parabolic distribution.

induction and this critical value for all three material systems is roughly at $B_3 = 0$ T.

As pointed out early in this paper, the proposed method can be also applied to the interfacial crack under non-uniform loadings on its faces. As an example, both linear and parabolic loadings are considered. It is assumed that the distribution of the loadings varies only along $x_1$-direction. Along $x_2$-direction, the applied loads are uniformly distributed. Since the crack length in $x_1$-direction is assumed to be $l = 1$ m, the distribution functions are given by

$$q(x_1) = \begin{cases} \frac{x_1}{0.5} q_0 & \text{for } 0 \leqslant x_1 \leqslant 0.5 \\ \frac{1-x_1}{0.5} q_0 & \text{for } 0.5 < x_1 \leqslant 1.0 \end{cases} \tag{39}$$

for linear distribution as shown in Fig. 12a and

$$q(x_1) = -q_0 x_1 (x_1 - 1) \quad \text{for } 0 \leqslant x_1 \leqslant 1.0 \tag{40}$$

for parabolic distribution as shown in Fig. 12(b), where $q_0$ is the strength of the applied loads. For comparison, the same loading strengths of $\sigma_{33}^0 = 40$ MPa, $D_3^0 = 0.01$ C/m$^2$ and $B_3^0 = 0.1$ T are considered for different loading distribution cases. Fig. 13 presents the distribution of the dimensionless $J$-integral along (a) the edge of $x_2 = 0$; and (b) the edge of $x_1 = 0$ of the square-shaped interfacial crack. It can be observed that the distribution of the $J$-integral along $x_1$-direction (Fig. 13a) for the linear distribution is similar to the one for the parabolic distribution but different from the one due to the uniform distribution. It is also seen from both Figs. 13a and 13b that the $J$-integral for the uniform distribution is the largest among all three cases and the one due to the parabolic distribution is the smallest. Besides, for both linear and parabolic distributed loadings, the maximum $J$-integral along $x_1$-direction (Fig. 13a) does not occur at the center of the edge, although no shear traction loadings are applied.

Figs. 14–16 show, respectively, the contour plots of the obtained opening displacement discontinuity, the electric potential discontinuity and the magnetic potential discontinuity distributed on the whole crack face under mixed loadings of (a) uniform distribution; (b) linear distribution; and (c) parabolic distribution. The loading conditions are exactly the same as the ones in Fig. 13. It is obvious that the distributions of these extended displacement discontinuities for the three different loading types are different.

## 7. Concluding remarks

Green's functions of constant extended interfacial displacement discontinuities within a rectangular element and of point extended interfacial displacement discontinuities in 3D transversely isotropic MEE bi-materials have been derived. Based on the obtained Green's functions, the extended displacement discontinuity boundary integral method has been developed to analyze the electrically and magnetically impermeable interfacial cracks in 3D MEE bi-materials. When the Dirac delta function and the unit Heaviside

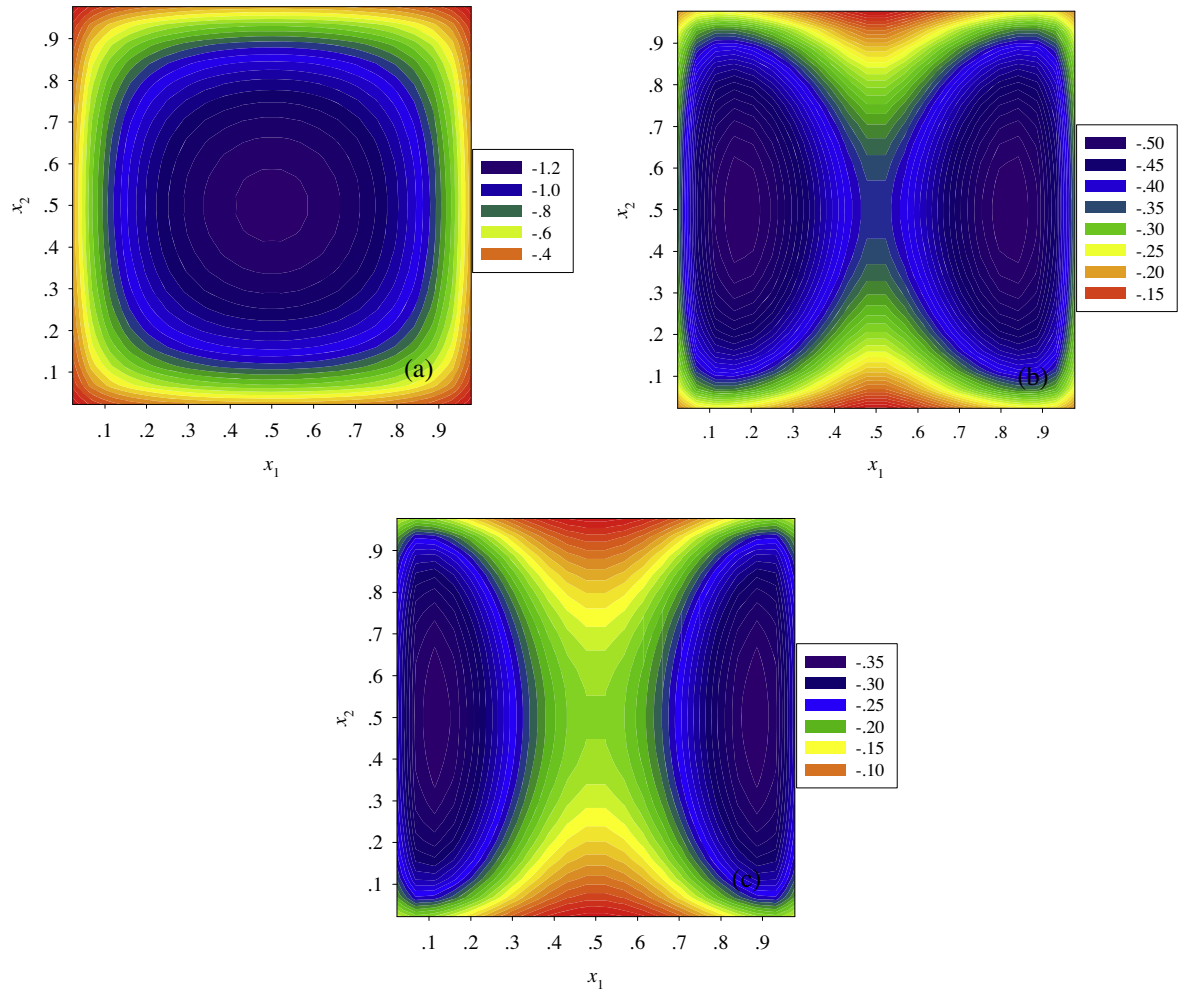


**Fig. 16.** Dimensionless magnetic potential jump $||\psi||$ ($\times 10^{-8}$) on the whole square interfacial crack under mixed loadings of (a) uniform distribution; (b) linear distribution; and (c) parabolic distribution.

function in the Green's functions are approximated, respectively, by the Gaussian distribution function and the Error function, the oscillatory singularities of the extended stresses near the interfacial crack front disappear. Thus, the singularity behaviors near the crack front of MEE bi-materials become the classical elastic one. The stress intensity factors, electric displacement intensity factor and magnetic induction intensity factor have been derived and expressed in terms of the extended displacement discontinuities. The effect of the parameter $\varepsilon$ in the Gaussian distribution function on the $J$-integral is proved to be very small within the given range of $\varepsilon$. This feature makes the developed extended displacement discontinuity method more efficient and useful for interfacial crack analysis in 3D MEE materials. Numerical results demonstrate the coupling effects on the stress intensity factors of different modes for the interfacial crack. Material mismatch on both sides of the interface also shows a significant effect on the crack parameters, so is the non-uniform loadings. It should be mentioned that the presented formulation is also applicable to interfacial crack problems in decoupled piezoelectric and/or elastic bi-materials as special cases.

## Acknowledgments

The work was supported by the National Natural Science Foundation of China (Nos. 11102186, 11272290, and 11172273), Science and Technology Research Projects of Henan Province (No. 132102210412), and Bairen Program in Henan Province.

## Appendix A. Constants $K_{ij}$ and $K_{zij}$ in Eqs. (8) and (9)

To calculate constants $K_{ij}$ and $K_{zij}$, three steps are needed as shown in the following:

A1. The material-related constants in deriving the fundamental solutions for a transversely isotropic MEE material are given below:

$$\begin{aligned}
&\alpha_{im} = k_{mi}s_i, \quad i = 1-4, \quad m = 1-3,\\
&\xi_i = (c_{13}\alpha_{i1} + e_{31}\alpha_{i2} + f_{31}\alpha_{i3})s_i - c_{12},\\
&\omega_{51} = c_{44}s_5, \quad \omega_{52} = e_{15}s_5, \quad \omega_{53} = f_{15}s_5,\\
&\vartheta_{i1} = (c_{33}\alpha_{i1} + e_{33}\alpha_{i2} + f_{33}\alpha_{i3})s_i - c_{13},\\
&\vartheta_{i2} = (e_{33}\alpha_{i1} - \kappa_{33}\alpha_{i2} - g_{33}\alpha_{i3})s_i - e_{31},\\
&\vartheta_{i3} = (f_{33}\alpha_{i1} - g_{33}\alpha_{i2} - \mu_{33}\alpha_{i3})s_i - f_{31},\\
&\omega_{i1} = c_{44}(s_i + \alpha_{i1}) + e_{15}\alpha_{i2} + f_{15}\alpha_{i3},\\
&\omega_{i2} = e_{15}(s_i + \alpha_{i1}) - \kappa_{11}\alpha_{i2} - g_{11}\alpha_{i3},\\
&\omega_{i3} = f_{15}(s_i + \alpha_{i1}) - g_{11}\alpha_{i2} - \mu_{11}\alpha_{i3},
\end{aligned} \tag{A1}$$

where $s_i$ are the roots of the material characteristic equation and $k_{mi}$ are the material-related constants given in Zhao et al. (2008a).

A2. Related coefficients in the fundamental solutions (Zhao et al., 2008a) are determined by

$$\begin{aligned}
&\sum_{i=1}^{4}A_i=0,\quad 4\pi\sum_{i=1}^{4}\vartheta_{i1}A_i=-1,\quad 4\pi\sum_{i=1}^{4}\vartheta_{i2}A_i=0,\quad 4\pi\sum_{i=1}^{4}\vartheta_{i3}A_i=0,\\
&A_i+\sum_{j=1}^{4}A_{ji}=\sum_{j=1}^{4}A_{ji}^L,\quad A_i\alpha_{im}-\sum_{j=1}^{4}A_{ji}\alpha_{jm}=\sum_{j=1}^{4}A_{ji}^L\alpha_{jm}^L,\\
&A_i\vartheta_{im}+\sum_{j=1}^{4}A_{ji}\vartheta_{jm}=\sum_{j=1}^{4}A_{ji}^L\vartheta_{jm}^L,\quad A_i\omega_{i1}-\sum_{j=1}^{4}A_{ji}\omega_{j1}=\sum_{j=1}^{4}A_{ji}^L\omega_{j1}^L,
\end{aligned}\tag{A2}$$

$$\begin{aligned}
&\sum_{i=1}^{4}B_i=0,\quad 4\pi\sum_{i=1}^{4}\vartheta_{i1}B_i=0,\quad 4\pi\sum_{i=1}^{4}\vartheta_{i2}B_i=1,\quad 4\pi\sum_{i=1}^{4}\vartheta_{i3}B_i=0,\\
&B_i+\sum_{j=1}^{4}B_{ji}=\sum_{j=1}^{4}B_{ji}^L,\quad B_i\alpha_{im}-\sum_{j=1}^{4}B_{ji}\alpha_{jm}=\sum_{j=1}^{4}B_{ji}^L\alpha_{jm}^L,\\
&B_i\vartheta_{im}+\sum_{j=1}^{4}B_{ji}\vartheta_{jm}=\sum_{j=1}^{4}B_{ji}^L\vartheta_{jm}^L,\quad B_i\omega_{i1}-\sum_{j=1}^{4}B_{ji}\omega_{j1}=\sum_{j=1}^{4}B_{ji}^L\omega_{j1}^L,
\end{aligned}\tag{A3}$$

$$\begin{aligned}
&\sum_{i=1}^{4}C_i=0,\quad 4\pi\sum_{i=1}^{4}\vartheta_{i1}C_i=0,\quad 4\pi\sum_{i=1}^{4}\vartheta_{i2}C_i=0,\quad 4\pi\sum_{i=1}^{4}\vartheta_{i3}C_i=1,\\
&C_i+\sum_{j=1}^{4}C_{ji}=\sum_{j=1}^{4}C_{ji}^L,\quad C_i\alpha_{im}-\sum_{j=1}^{4}C_{ji}\alpha_{jm}=\sum_{j=1}^{4}C_{ji}^L\alpha_{jm}^L,\\
&C_i\vartheta_{im}+\sum_{j=1}^{4}C_{ji}\vartheta_{jm}=\sum_{j=1}^{4}C_{ji}^L\vartheta_{jm}^L,\quad C_i\omega_{i1}-\sum_{j=1}^{4}C_{ji}\omega_{j1}=\sum_{j=1}^{4}C_{ji}^L\omega_{j1}^L,
\end{aligned}\tag{A4}$$

$$\begin{aligned}
&\sum_{i=1}^{4}\alpha_{im}D_i=0,\quad s_5D_5+\sum_{i=1}^{4}s_iD_i=0,\\
&2\pi c_{44}s_5D_5-2\pi\sum_{i=1}^{4}\omega_{i1}D_i=-1,\quad D_5+D_{55}=D_{55}^L,\\
&\alpha_{im}D_i-\sum_{j=1}^{4}\alpha_{jm}D_{ji}=\sum_{j=1}^{4}\alpha_{jm}^LD_{ji}^L,\quad D_i+\sum_{j=1}^{4}D_{ji}=\sum_{j=1}^{4}D_{ji}^L,\\
&\omega_{51}(D_{55}-D_5)=-\omega_{51}^LD_{55}^L,\\
&\omega_{i1}D_i-\sum_{j=1}^{4}\omega_{j1}D_{ji}=\sum_{j=1}^{4}\omega_{j1}^LD_{ji}^L,\\
&\vartheta_{im}D_i+\sum_{j=1}^{4}\vartheta_{jm}D_{ji}=\sum_{j=1}^{4}\vartheta_{jm}^LD_{jm}^L.
\end{aligned}\tag{A5}$$

In the above equations, the variables with the superscript "$L$" denote the material constants in the lower half space.

A3. Constants appearing in Eqs. (8) and (9) are calculated as

$$\begin{aligned}
K_{11}&=c_{44}\omega_{51}(D_5-D_{55})s_5\\
&\quad+2\sum_{i=1}^{4}\omega_{i1}\left[c_{44}\left(D_is_i-\sum_{j=1}^{4}D_{ij}s_j\right)+c_{44}\left(A_i-\sum_{j=1}^{4}A_{ij}\right)\right.\\
&\quad\left.-e_{15}\left(B_i-\sum_{j=1}^{4}B_{ij}\right)-f_{15}\left(C_i-\sum_{j=1}^{4}C_{ij}\right)\right],\\
K_{12}&=-2c_{44}\omega_{51}(D_5-D_{55})s_5\\
&\quad-\sum_{i=1}^{4}\omega_{i1}\left[c_{44}\left(D_is_i-\sum_{j=1}^{4}D_{ij}s_j\right)+c_{44}\left(A_i-\sum_{j=1}^{4}A_{ij}\right)\right.\\
&\quad\left.-e_{15}\left(B_i-\sum_{j=1}^{4}B_{ij}\right)-f_{15}\left(C_i-\sum_{j=1}^{4}C_{ij}\right)\right],
\end{aligned}\tag{A6}$$

$$\begin{aligned}
&K_{41}=\sum_{i=1}^{4}\vartheta_{i1}K_j^L,\quad K_{42}=\sum_{i=1}^{4}\vartheta_{i2}K_j^L,\quad K_{43}=\sum_{i=1}^{4}\vartheta_{i3}K_j^L,\\
&K_j^L=-c_{44}\left(D_is_i+\sum_{j=1}^{4}D_{ij}s_j\right)-c_{44}\left(A_i+\sum_{j=1}^{4}A_{ij}\right)\\
&\qquad+e_{15}\left(B_i+\sum_{j=1}^{4}B_{ij}\right)+f_{15}\left(C_i+\sum_{j=1}^{4}C_{ij}\right),
\end{aligned}\tag{A7}$$

$$\begin{aligned}
K_1&=\sum_{i=1}^{4}\omega_{i1}\left[c_{13}\left(D_i-\sum_{j=1}^{4}D_{ij}\right)-c_{33}\left(A_is_i-\sum_{j=1}^{4}A_{ij}s_j\right)\right.\\
&\quad\left.+e_{33}\left(B_is_i-\sum_{j=1}^{4}B_{ij}s_j\right)+f_{33}\left(C_is_i-\sum_{j=1}^{4}C_{ij}s_j\right)\right],\\
K_2&=\sum_{i=1}^{4}\omega_{i1}\left[e_{31}\left(D_i-\sum_{j=1}^{4}D_{ij}\right)-e_{33}\left(A_is_i-\sum_{j=1}^{4}A_{ij}s_j\right)\right.\\
&\quad\left.-\kappa_{33}\left(B_is_i-\sum_{j=1}^{4}B_{ij}s_j\right)-g_{33}\left(C_is_i-\sum_{j=1}^{4}C_{ij}s_j\right)\right],\\
K_3&=\sum_{i=1}^{4}\omega_{i1}\left[f_{31}\left(D_i-\sum_{j=1}^{4}D_{ij}\right)-f_{33}\left(A_is_i-\sum_{j=1}^{4}A_{ij}s_j\right)\right.\\
&\quad\left.-g_{33}\left(B_is_i-\sum_{j=1}^{4}B_{ij}s_j\right)-\mu_{33}\left(C_is_i-\sum_{j=1}^{4}C_{ij}s_j\right)\right],
\end{aligned}\tag{A8}$$

$$\begin{aligned}
&K_{z11}=\sum_{i=1}^{4}\vartheta_{i1}K_{zz1},\quad K_{z21}=\sum_{i=1}^{4}\vartheta_{i2}K_{zz1},\quad K_{z31}=\sum_{i=1}^{4}\vartheta_{i3}K_{zz1},\\
&K_{z12}=\sum_{i=1}^{4}\vartheta_{i1}K_{zz2},\quad K_{z22}=\sum_{i=1}^{4}\vartheta_{i2}K_{zz2},\quad K_{z32}=\sum_{i=1}^{4}\vartheta_{i3}K_{zz2},\\
&K_{z13}=\sum_{i=1}^{4}\vartheta_{i1}K_{zz3},\quad K_{z23}=\sum_{i=1}^{4}\vartheta_{i2}K_{zz3},\quad K_{z33}=\sum_{i=1}^{4}\vartheta_{i3}K_{zz3},
\end{aligned}\tag{A9}$$

where

$$\begin{aligned}
K_{zz1}&=c_{13}\left(D_i+\sum_{j=1}^{4}D_{ij}\right)-c_{33}\left(A_is_i+\sum_{j=1}^{4}A_{ij}s_j\right)\\
&\quad+e_{33}\left(B_is_i+\sum_{j=1}^{4}B_{ij}s_j\right)+f_{33}\left(C_is_i+\sum_{j=1}^{4}C_{ij}s_j\right),\\
K_{zz2}&=e_{31}\left(D_i+\sum_{j=1}^{4}D_{ij}\right)-e_{33}\left(A_is_i+\sum_{j=1}^{4}A_{ij}s_j\right)\\
&\quad-\varepsilon_{33}\left(B_is_i+\sum_{j=1}^{4}B_{ij}s_j\right)-g_{33}\left(C_is_i+\sum_{j=1}^{4}C_{ij}s_j\right),\\
K_{zz3}&=f_{31}\left(D_i+\sum_{j=1}^{4}D_{ij}\right)-f_{33}\left(A_is_i+\sum_{j=1}^{4}A_{ij}s_j\right)\\
&\quad-g_{33}\left(B_is_i+\sum_{j=1}^{4}B_{ij}s_j\right)-\mu_{33}\left(C_is_i+\sum_{j=1}^{4}C_{ij}s_j\right).
\end{aligned}\tag{A10}$$

## Appendix B. Calculation of divergent integrals $I_1$ in Eq. (13)

To calculate the divergent integral $I_1$ in Eq. (13) or Eq. (16), the rectangular integration area is divided into eight triangular areas, as shown in Fig. 3. The finite part integral $I_1$ is evaluated over each triangle using Eq. (17). Note that $f(\theta)=\cos^2\theta$ for $I_1$.

For triangle ①:

$$R(\theta) = \frac{b + x_2}{\cos(\pi/2 + \theta)},$$
$$I_1^1 = -\int_{-\pi/2}^{-\theta_2} \frac{\cos^2\theta}{R(\theta)} d\theta = -\frac{1}{b + x_2}\frac{1}{3}\cos^3\theta_2. \tag{B1}$$

For triangles ② and ③:

$$R(\theta) = \frac{a - x_1}{\cos\theta},$$
$$I_1^{2+3} = -\int_{-\theta_2}^{\theta_3} \frac{\cos^2\theta}{R(\theta)} d\theta = -\frac{1}{a - x_1}\left(\frac{3}{4}\sin\theta_3 + \frac{1}{12}\sin 3\theta_3 + \frac{3}{4}\sin\theta_2 + \frac{1}{12}\sin 3\theta_2\right). \tag{B2}$$

For triangle ④:

$$R(\theta) = \frac{b - x_2}{\cos(\pi/2 - \theta)},$$
$$I_1^4 = -\int_{\theta_3}^{\pi/2} \frac{\cos^2\theta}{R(\theta)} d\theta = -\frac{1}{b - x_2}\frac{1}{3}\cos^3\theta_3. \tag{B3}$$

For triangle ⑤:

$$R(\theta) = \frac{b - x_2}{\cos(\theta - \pi/2)},$$
$$I_1^5 = -\int_{\pi/2}^{\pi/2+\theta_5} \frac{\cos^2\theta}{R(\theta)} d\theta = -\frac{1}{b - x_2}\frac{1}{3}\sin^3\theta_5. \tag{B4}$$

For triangle ⑥ + ⑦:

$$R(\theta) = \frac{a + x_1}{\cos(\pi - \theta)},$$
$$I_1^{6+7} = -\int_{\pi/2+\theta_5}^{\pi+\theta_7} \frac{\cos^2\theta}{R(\theta)} d\theta = -\frac{1}{a + x_1}\left(\frac{3}{4}\sin\theta_7 + \frac{1}{12}\sin 3\theta_7 + \frac{3}{4}\cos\theta_5 - \frac{1}{12}\cos 3\theta_5\right). \tag{B5}$$

For triangle ⑧:

$$R(\theta) = \frac{b + x_2}{\cos(3\pi/2 - \theta)},$$
$$I_1^8 = -\int_{\pi+\theta_7}^{3\pi/2} \frac{\cos^2\theta}{R(\theta)} d\theta = -\frac{1}{b + x_2}\frac{1}{3}\cos^3\theta_7. \tag{B6}$$

Adding all the results in Eqs. (B1)–(B6), we obtain

$$\begin{aligned} I_1 = &-\frac{1}{b + x_2}\frac{1}{3}\cos^3\theta_2 - \frac{1}{b - x_2}\frac{1}{3}\cos^3\theta_3 \\ &-\frac{1}{a - x_1}\left(\frac{3}{4}\sin\theta_3 + \frac{1}{12}\sin 3\theta_3 + \frac{3}{4}\sin\theta_2 + \frac{1}{12}\sin 3\theta_2\right) \\ &-\frac{1}{b - x_2}\frac{1}{3}\sin^3\theta_5 - \frac{1}{b + x_2}\frac{1}{3}\cos^3\theta_7 \\ &-\frac{1}{a + x_1}\left[\frac{3}{4}\sin\theta_7 + \frac{1}{12}\sin 3\theta_7 + \frac{3}{4}\cos\theta_5 - \frac{1}{12}\cos 3\theta_5\right]. \end{aligned} \tag{B7}$$

From the geometric relation in Fig. 3, the sine and cosine expressions for angles $\theta_2$, $\theta_3$, $\theta_5$ and $\theta_7$ are presented as

$$\begin{aligned} \cos\theta_2 &= \frac{a - x_1}{\sqrt{(a - x_1)^2 + (b + x_2)^2}}, & \sin\theta_2 &= \frac{b + x_2}{\sqrt{(a - x)^2 + (b + x_2)^2}}; \\ \cos\theta_3 &= \frac{a - x_1}{\sqrt{(a - x_1)^2 + (b - x_2)^2}}, & \sin\theta_3 &= \frac{b - x_2}{\sqrt{(a - x)^2 + (b - x_2)^2}}; \\ \cos\theta_5 &= \frac{b - y}{\sqrt{(a + x_1)^2 + (b - x_2)^2}}, & \sin\theta_5 &= \frac{a + x_1}{\sqrt{(a + x)^2 + (b - x_2)^2}}; \\ \cos\theta_7 &= \frac{a + x_1}{\sqrt{(a + x_1)^2 + (b + x_2)^2}}, & \sin\theta_7 &= \frac{b + x_2}{\sqrt{(a + x_1)^2 + (b + x_2)^2}}. \end{aligned} \tag{B8}$$

Besides, we have the following formulas

$$\begin{aligned} \cos 3\theta &= \cos^3\theta - 3\sin^2\theta\cos\theta, \\ \sin 3\theta &= 3\sin\theta\cos^2\theta - \sin^3\theta. \end{aligned} \tag{B9}$$

Finally, $I_1$ is calculated as

$$\begin{aligned} I_1(x_1, x_2, a, b) = &-\frac{(x_1 - a)^2 + 2(x_2 - b)^2}{3(x_1 - a)(x_2 - b)\sqrt{(x_1 - a)^2 + (x_2 - b)^2}} \\ &+\frac{(x_1 - a)^2 + 2(x_2 + b)^2}{3(x_1 - a)(x_2 + b)\sqrt{(x_1 - a)^2 + (x_2 + b)^2}} \\ &+\frac{(x_1 + a)^2 + 2(x_2 - b)^2}{3(x_1 + a)(x_2 - b)\sqrt{(x_1 + a)^2 + (x_2 - b)^2}} \\ &-\frac{(x_1 + a)^2 + 2(x_2 + b)^2}{3(x_1 + a)(x_2 + b)\sqrt{(x_1 + a)^2 + (x_2 + b)^2}}. \end{aligned} \tag{B10}$$

The expression of $I_1$ in Eq. (B10) is the same as the one in Eq. (14a). Similarly, $I_2$ and $I_3$ can also be calculated with the results being exactly the same as those in Eqs. (14b) and (14c).

## Appendix C. Derivation of matrix *Y* for *J*-integral

The standard eigenequation for MEE material is given as (Zhao and Fan, 2008):

$$\begin{pmatrix} \mathbf{N}_1 & \mathbf{N}_2 \\ \mathbf{N}_3 & \mathbf{N}_1^T \end{pmatrix}\begin{pmatrix} \mathbf{a} \\ \mathbf{b} \end{pmatrix} = p\begin{pmatrix} \mathbf{a} \\ \mathbf{b} \end{pmatrix}, \tag{C1}$$

where $\mathbf{N}_1 = -\mathbf{T}^{-1}\mathbf{R}^T$, $\mathbf{N}_2 = \mathbf{T}^{-1} = \mathbf{N}_2^T$, $\mathbf{N}_3 = \mathbf{R}\mathbf{T}^{-1}\mathbf{R}^T - \mathbf{Q} = \mathbf{N}_3^T$ and

$$\mathbf{Q} = \begin{pmatrix} c_{i1k1} & e_{11i} & f_{11i} \\ e_{11i}^T & -\kappa_{11} & -g_{11} \\ f_{11i}^T & -g_{11} & -\mu_{11} \end{pmatrix}, \quad \mathbf{R} = \begin{pmatrix} c_{i1k2} & e_{21i} & f_{21i} \\ e_{12i}^T & -\kappa_{12} & -g_{12} \\ f_{12i}^T & -g_{12} & -\mu_{12} \end{pmatrix},$$
$$\mathbf{T} = \begin{pmatrix} c_{i2k2} & e_{22i} & f_{22i} \\ e_{22i}^T & -\kappa_{22} & -g_{22} \\ f_{22i}^T & -g_{22} & -\mu_{22} \end{pmatrix}.$$

Letting matrices $\mathbf{A} = (\boldsymbol{a}_1, \boldsymbol{a}_2, \boldsymbol{a}_3, \boldsymbol{a}_4, \boldsymbol{a}_5)$ and $\mathbf{B} = (\boldsymbol{b}_1, \boldsymbol{b}_2, \boldsymbol{b}_3, \boldsymbol{b}_4, \boldsymbol{b}_5)$ with $\boldsymbol{a}_\alpha$ and $\boldsymbol{b}_\alpha$ being the eigenvectors of Eq. (C1), we then have:

$$\begin{aligned} \mathbf{A}\mathbf{A}^T + \overline{\mathbf{A}\mathbf{A}^T} &= \mathbf{B}\mathbf{B}^T + \overline{\mathbf{B}\mathbf{B}^T} = \mathbf{0}, \\ \mathbf{B}\mathbf{A}^T + \overline{\mathbf{B}\mathbf{A}^T} &= \mathbf{A}\mathbf{B}^T + \overline{\mathbf{A}\mathbf{B}^T} = \mathbf{I}, \end{aligned} \tag{C2}$$

where $\mathbf{I}$ is a $5 \times 5$ identity matrix. The matrix $\mathbf{Y}$ in the calculations of *J*-integral is defined by

$$\mathbf{Y} = i\mathbf{A}\mathbf{B}^{-1}. \tag{C3}$$

## Appendix D. Material constants

| | $c_{11}$ | $c_{33}$ | $c_{12}$ | $c_{13}$ | $c_{44}$ | $e_{31}$ | $e_{33}$ | $e_{15}$ |
|---|---|---|---|---|---|---|---|---|
| $BaTiO_3$ | 166 | 162 | 77 | 78 | 43 | −4.4 | 18.6 | 11.6 |
| $CoFe_2O_4$ | 286 | 269.5 | 173 | 170.5 | 45.3 | 0 | 0 | 0 |

| | $\kappa_{11}$ | $\kappa_{33}$ | $\mu_{11}$ | $\mu_{33}$ | $f_{31}$ | $f_{33}$ | $f_{15}$ |
|---|---|---|---|---|---|---|---|
| $BaTiO_3$ | 11.2 | 12.6 | 5000 | 10,000 | 0 | 0 | 0 |
| $CoFe_2O_4$ | 0.08 | 0.093 | 59,000 | 157,000 | 580.3 | 699.7 | 550 |

(Units: $c_{ij}$ ($\times 10^9$ N/m$^2$); $e_{ij}$ (C/m$^2$); $\kappa_{ij}$ ($\times 10^{-9}$ C/Vm); $\mu_{ij}$ ($\times 10^{-9}$ Ns$^2$ C$^2$); $f_{ij}$ ($\times 10^{-9}$ N/Am)).

## References


Antipov, Y.A., 1999. An exact solution of the 3-D-problem of an interface semi-infinite plane crack. J. Mech. Phys. Solids 47, 1051–1093.

Atkinson, C., 1977. On stress singularities and interfaces in linear elastic fracture mechanics. Int. J. Fract. 13, 807–820.

Beom, H.G., Atluri, S.N., 1996. Near-tip fields and intensity factors for interfacial cracks in dissimilar anisotropic piezoelectric media. Int. J. Fract. 75, 163–183.

Bercial-Velez, J.P., Antipov, Y.A., Movchan, A.B., 2005. High-order asymptotics and perturbation problems for 3D interfacial cracks. J. Mech. Phys. Solids 53, 1128–1162.

Chue, C.H., Liu, T.J.C., 2005. Magneto-electro-elastic antiplane analysis of a bimaterial $BaTiO_3$–$CoFe_2O_4$ composite wedge with an interface crack. Theor. Appl. Fract. Mech. 44, 275–296.

Comninou, M., 1977. The interface crack. J. Appl. Mech. ASME 44, 631–636.

Comninou, M., 1990. An overview of interface cracks. Eng. Fract. Mech. 37, 197–208.

Crouch, S.L., 1976. Solution of plane elasticity problems by the displacement discontinuity method. I. Infinite body solution. Int. J. Numer. Methods Eng. 10, 301–343.

Cruse, T.A., 1996. BIE fracture mechanics analysis: 25 years of developments. Comput. Mech. 18, 1–11.

Ding, H.J., Jiang, A.M., Hou, P.H., Chen, W.Q., 2005. Green's functions for two-phase transversely isotropic magneto-electro-elastic media. Eng. Anal. Bound. Elem. 29, 551–561.

Dundurs, J., Gautesen, A.K., 1988. An opportunistic analysis of the interface crack. Int. J. Fract. 36, 151–159.

England, A.H., 1965. A crack between dissimilar media. J. Appl. Mech. 32, 400–402.

Erdogan, F., 1965. Stress distribution in bonded dissimilar materials with cracks. J. Appl. Mech. 32, 403–410.

Eshelby, J.D., 1951. The force on an elastic singularity. Philos. Trans. R. Soc. Lond. Ser. A Math. Phys. Sci. 244, 87–112.

Gao, C.F., Tong, P., Zhang, T.Y., 2003. Interfacial crack problems in magneto-electroelastic solids. Int. J. Eng. Sci. 41, 2105–2121.

Gao, C.F., Tong, P., Zhang, T.Y., 2004. Fracture mechanics for a mode III crack in a magnetoelectroelastic solid. Int. J. Solids Struct. 41, 6613–6629.

Hadamard, J., 1923. Lectures on Cauchy's Problem in Linear Partial Differential Equations, Dover Phoenix ed. Dover Publications, New York.

Herrmann, K.P., Loboda, V.V., 2000. Fracture-mechanical assessment of electrically permeable interface cracks in piezoelectric bimaterials by consideration of various contact zone models. Arch. Appl. Mech. 70, 127–143.

Hu, K., Chen, Z., 2014. An interface crack moving between magnetoelectroelastic and functionally graded elastic layers. Appl. Math. Model. 38, 910–925.

Huang, J.H., Chiu, Y.H., Liu, H.K., 1998. Magneto-electro-elastic Eshelby tensors for a piezoelectric–piezomagnetic composite reinforced ellipsoidal inclusions. J. Appl. Phys. 83, 5364–5370.

Ioakimidis, N.I., 1982. Application of finite-part integrals to the singular integral equations of crack problems in plane and three-dimensional elasticity. Acta Mech. 45, 31–47.

Kuo, C.M., Barnett, D.M., 1991. Stress singularities of interfacial cracks in bounded piezoelectric half-spaces. In: Wu, J.J., Ting, T.C.T., Barnett, D.M. (Eds.), Modern Theory of Anisotropic Elasticity and Applications. SIAM Proceedings Series, Philadelphia, pp. 33–50.

Lazarus, V., Leblond, J.B., 1998a. Three-dimensional crack-face weight functions for the semi-infinite interface crack-I: variation of the stress intensity factors due to some small perturbation of the crack front. J. Mech. Phys. Solids 46, 489–511.

Lazarus, V., Leblond, J.B., 1998b. Three-dimensional crack-face weight functions for the semi-infinite interface crack-II: integrodifferential equations on the weight functions and resolution. J. Mech. Phys. Solids 46, 513–536.

Noda, N.A., Kihara, T.A., 2002. Variation of the stress intensity factor along the front of a 3-D rectangular crack subjected to mixed-mode load. Arch. Appl. Mech. 72, 599–614.

Pan, E., 2002. Three-dimensional Green's functions in anisotropic magneto-electro-elastic bimaterials. J. Appl. Math. Phys. 53, 815–838.

Pan, E., Yuan, F.G., 2000. Boundary element analysis of three-dimensional cracks in anisotropic solids. Int. J. Numer. Methods Eng. 48, 211–237.

Pindra, N., Lazarus, V., Leblond, J.B., 2008. The deformation of the front of a 3D interface crack propagating quasistatically in a medium with random fracture properties. J. Mech. Phys. Solids 56, 1269–1295.

Qin, Q.H., Mai, Y.W., 1999. A closed crack tip model for interface cracks in thermopiezoelectric materials. Int. J. Solids Struct. 36, 2463–2479.

Qu, J., Li, Q., 1991. Interfacial dislocation and its applications to interface cracks in anisotropic bimaterials. J. Elast. 26, 169–195.

Rice, J.R., Sih, G.C., 1965. Plane problems of cracks in dissimilar media. J. Appl. Mech. 32, 418–423.

Schmitz, H., Volk, K., Wendland, W., 1993. Three-dimensional singularities of elastic fields near vertices. Numer. Methods Partial Differ. Equ. 9, 323–337.

Sih, G.C., Song, Z.F., 2003. Magnetic and electric poling effects associated with crack growth in $BaTiO_3$–$CoFe_2O_4$ composite. Theor. Appl. Fract. Mech. 39, 209–227.

Song, Z.F., Sih, G.C., 2003. Crack initiation behavior in magnetoelectroelastic composite under in-plane deformation. Theor. Appl. Fract. Mech. 39, 189–207.

Spyropoulos, C.P., Sih, G.C., Song, Z.F., 2003. Magnetoelectroelastic composite with poling parallel to plane of line crack under out-of-plane deformation. Theor. Appl. Fract. Mech. 39, 281–289.

Suo, Z., Hutchinson, J.W., 1990. Interface crack between two elastic layers. Int. J. Fract. 43, 1–18.

Suo, Z., Kuo, C.M., Barnett, D.M., Willis, J.R., 1992. Fracture mechanics for piezoelectric ceramics. J. Mech. Phys. Solids 40, 739–765.

Tian, W.Y., Gabbert, U., 2005. Parallel crack near the interface of magnetoelectroelastic bimaterials. Comput. Mater. Sci. 32, 562–567.

Van Run, A.M.J.G., Terrell, D.R., Scholing, J.H., 1974. An in situ grown eutectic magnetoelectric composite material. J. Mater. Sci. 9, 1710–1714.

Wang, B.L., Mai, Y.W., 2003. Crack tip field in piezoelectric/piezomagnetic media. Eur. J. Mech. A Solid 22, 591–602.

Wang, B.L., Mai, Y.W., 2007. Applicability of the crack-face electromagnetic boundary conditions for fracture of magnetoelectroelastic materials. Int. J. Solids Struct. 44, 387–398.

Wang, X.M., Shen, Y.P., 1996. The conservation laws and path-independent integrals with an application for linear electro-magneto-elastic media. Int. J. Solids Struct. 33, 865–878.

Wang, Q., Noda, N.A., Honda, M.A., Chen, M.C., 2001. Variation of stress intensity factor along the front of a 3D rectangular crack by using a singular integral equation method. Int. J. Fract. 108, 119–131.

Williams, M.L., 1959. The stress around a fault or crack in dissimilar media. Bull. Seismol. Soc. Am. 49, 199–204.

Willis, J.R., 1971. Fracture mechanics of interfacial cracks. J. Mech. Phys. Solids 19, 353–368.

Zhang, A.B., Wang, B.L., 2013. An opportunistic analysis of the interface crack based on the modified interface dislocation method. Int. J. Solids Struct. 50, 15–20.

Zhang, T.Y., Zhao, M.H., Tong, P., 2002. Fracture of piezoelectric ceramics. Adv. Appl. Mech. 38, 147–289.

Zhao, M.H., Fan, C.Y., 2008. Strip electric–magnetic breakdown model in magnetoelectroelastic medium. J. Mech. Phys. Solids 56, 3441–3458.

Zhao, M.H., Shen, Y.P., Liu, Y.J., Liu, G.N., 1997. Isolated crack in three-dimensional piezoelectric solid: Part II – stress intensity factors for circular crack. Theor. Appl. Fract. Mech. 26, 141–149.

Zhao, M.H., Fan, C.Y., Yang, F., Liu, T., 2007. Analysis method of planar cracks of arbitrary shape in the isotropic plane of a three-dimensional transversely isotropic magnetoelectroelastic medium. Int. J. Solids Struct. 44, 4505–4523.

Zhao, M.H., Li, N., Fan, C.Y., 2008a. Solution method of interface cracks in three-dimensional transversely isotropic piezoelectric bimaterials. Eng. Anal. Bound. Elem. 32, 545–555.

Zhao, M.H., Li, N., Fan, C.Y., Xu, G.T., 2008b. Analysis method of planar interface cracks of arbitrary shape in three-dimensional transversely isotropic magnetoelectroelastic bimaterials. Int. J. Solids Struct. 45, 180–1824.

Zhao, Y.F., Zhao, M.H., Pan, E., Fan, C.Y., 2014. Analysis of an interfacial crack in a piezoelectric bi-material via the extended Green's functions and displacement discontinuity method. Int. J. Solids Struct. 51, 1456–1463.

Zhong, X.C., Li, X.F., 2006. A finite length crack propagating along the interface of two dissimilar magnetoelectroelastic materials. Int. J. Eng. Sci. 44, 1394–1407.

Zhou, A.G., Wang, B., Sun, Y.G., 2004. Two collinear interface cracks in magneto-electro-elastic composites. Int. J. Eng. Sci. 42, 1155–1167.

Zhu, B.J., Shi, Y.L., Qin, T.Y., Sukop, M., Yu, S.H., Li, Y.B., 2009. Mixed-mode stress intensity factors of 3D interface crack in fully coupled electromagnetothermoelastic multiphase composites. Int. J. Solids Struct. 46, 2669–2679.